***TITLE***

# Melanocyte differentiation and mechanosensation are differentially modulated by distinct extracellular matrix proteins

***AUTHORS***

Carole Luthold[1,2,3*], Marie Didion[1,2,3], Emilio Benedum[1,2,3], Ann-Kathrin Burkhart[1,2,3], Nina Demmerle[1,2,3], Gubesh Gunaratnam[4], Vanessa Samira Rácz[1,2,3], Markus Bischoff[4], Annika Ridzal[1,3], and Sandra Iden[1,2,3*]

***AFFILIATIONS***

[1] Cell & Developmental Biology, Saarland University, Faculty of Medicine, Homburg/Saar, Germany

[2] Center for Gender-specific Biology & Medicine (CGBM), Saarland University, Faculty of Medicine, Homburg/Saar, Germany

[3] Center for Human & Molecular Biology (ZHMB), Saarland University, Germany

[4] Institute of Medical Microbiology & Hygiene, Homburg/Saar, Germany

***CONTACT DETAILS***

CL, SI: Cell & Developmental Biology, Saarland University, Faculty of Medicine, Kirrberger Strasse, Building 61.4, 66421 Homburg/Saar, Germany

****CORRESPONDENCE***

carole.luthold@uni-saarland.de, sandra.iden@uks.eu

***ORCIDs***

CL: 0009-0009-9297-7516

MD: 0009-0008-4114-8841

EB: 0009-0006-0751-6087

AKB: 0000-0003-4128-6677

ND: 0009-0007-4436-3048

GG: 0000-0002-6533-8681

VSR: 0009-0007-4884-1051

MB: 0000-0001-6734-2732

AR: 0000-0002-9038-0734

SI: 0000-0003-2333-9827

***RUNNING TITLE*** ECM molecules and substrate stiffness steer melanocyte functions

***WORD COUNT*** 4574 (abstract, introduction, results, discussion, conclusion)

***DISPLAY ITEMS*** 6 Figures, 4 Supplementary Figures, 2 Supplementary Tables

***ABSTRACT***

Dysfunctions in melanocytes can lead to pigmentation disorders, such as albinism, or contribute to the development of melanoma, the most aggressive form of skin cancer. Epidermal melanocytes typically interact with the collagen IV-rich basement membrane, but upon injury or in pathological conditions, they can encounter environments rich in collagen I or fibronectin. While alterations in ECM composition and stiffness are known to impact cell behavior, the specific roles of each of these cues for melanocyte functions remain unclear. To explore the impact of these extrinsic cues, we here exposed murine melanocytes to different ECM proteins as well as varying substrate stiffnesses. This study identified MITF, a key regulator of melanocyte differentiation and function, as an ECM- and mechanosensitive transcription factor. We further revealed that distinct ECM proteins and substrate stiffness engage a MEK/ERK/MITF signaling axis to control melanocyte functions. Exposure of melanocytes to collagen I restricted ERK activation, promoting high nuclear MITF levels associated with melanocyte proliferation and differentiation. Conversely, fibronectin elicited elevated ERK activation, leading to low nuclear MITF, correlating with a dedifferentiated and motile phenotype. Importantly, inhibiting ERK activity in melanocytes cultured on fibronectin led to increased MITF nuclear localization, MITF target gene expression and enhanced melanogenesis. Additionally, we uncovered that melanocyte mechanoresponses differ depending on the specific ECM environment. Together, these findings reveal a synergistic effect of extrinsic cues on melanocyte function, with a context-dependent MITF regulation downstream of ERK, offering new perspectives for our understanding of melanocyte-related pathologies.

***KEYWORDS***

Melanocytes; MITF; Differentiation; Extracellular matrix; Type I Collagen; Fibronectin; Stiffness; ERK signaling; Melanogenesis; Mechanosensation.

## *INTRODUCTION*

Melanocytes (MCs) are pigment-producing cells found in the basal layer of the skin epidermis, and in various organs such as the brain, heart, and eyes (Centeno et al., 2023). The pronounced dendritic morphology of cutaneous MCs enables an efficient melanosome transfer to surrounding keratinocytes, providing photoprotection (Benito-Martínez et al., 2021; Cui & Man, 2023; Domingues et al., 2020; Hirobe, 2014; Prospéri et al., 2024). Dysfunctions of MCs can cause pigmentation disorders such as albinism and vitiligo (Coutant et al., 2024), and can lead to malignant transformation into melanoma, an aggressive form of skin cancer responsible for most skin cancer-related deaths (Matthews et al., 2017).

The specification and differentiation of MCs from the neural lineage are governed by the melanocyte-inducing transcription factor (MITF). MITF regulates MC differentiation by controlling the expression of pigmentation genes (e.g., *Tyr*, *Trp1*, *Trp2*) and maintains cellular homeostasis by modulating genes involved, among others, in cell-cycle progression (e.g., *Cdk2*) and apoptosis (e.g., *Bcl2*) (Goding & Arnheiter, 2019; Kawakami & Fisher, 2017). MITF is also a major player of melanoma progression, influencing both, the melanoma cell differentiation state and plasticity, contributing to high tumor heterogeneity. Within a single tumor, different cell states co-exist: highly differentiated, proliferative melanocytic cells, which are associated with high MITF levels, whereas slow-cycling, dedifferentiated, invasive stem-like cells correlate with low MITF levels (Arozarena & Wellbrock, 2019; Carreira et al., 2006; Cheli et al., 2011; Hoek et al., 2008; Müller et al., 2014; Popovic & Tartare-Deckert, 2022; Rambow et al., 2019; Tirosh et al., 2016; Tsoi et al., 2018; Wouters et al., 2020). Interestingly, differentiated MCs can give rise to melanoma through a process that includes their reprograming and dedifferentiation (Köhler et al., 2017). However, the specific factors and mechanisms driving this dedifferentiation of mature MCs, and the role of MITF in these processes, remain poorly understood. Therefore, understanding how MITF affects MC plasticity and identifying novel factors that regulate MITF expression and activity could provide new insights into the mechanisms underlying MC transformation.

In addition to the heterotypic cell-cell interaction with keratinocytes, MCs are in direct contact with the basement membrane, a specialized extracellular matrix (ECM) rich in type IV collagen (COL IV), which forms the junction with the underlying dermis, comprising type I collagen (COL I) and fibronectin (FN) (Pfisterer et al., 2021). This implies that under physiological conditions, COL IV is the predominant ECM type epidermal MCs are exposed to, whereas interactions with dermal COL I and FN can occur due to altered basement membrane integrity, for instance, following injury or chronic UV exposure (Amano, 2009, 2016; Fisher & Rittié, 2018; Iriyama et al., 2011, 2020; Yoshihisa et al., 2014). Within the skin, a wide range of stiffness has been reported for different compartments, ranging from lower kPa (dermis-like) to lower MPa

(epidermis-like) values (Biggs et al., 2020; Feng et al., 2022; Graham et al., 2019). Importantly, the cellular microenvironment, including ECM components and tissue stiffness, significantly impacts cell fate and function (Bonnans et al., 2014; Guilak et al., 2009; Walma & Yamada, 2020). Cells adapt to these molecular and mechanical parameters by transmitting environmental signals to intracellular signal transduction pathways, including MAPK/ERK pathways (Tan et al., 2023). Crucial for this process are focal adhesions (FAs), dynamic multi-protein complexes at the plasma membrane that link the ECM to the actin cytoskeleton via transmembrane receptors such as integrins. Notably, focal adhesion kinase (FAK), a key signaling protein within FAs, is activated through integrin engagement with the ECM, resulting in autophosphorylation and activation of downstream signaling pathways like MAPK/ERK (Paszek et al., 2005). In various cell systems, such signal activation downstream of ECM cues has been reported to affect the localization and activation levels of various transcription factors and coregulatory factors, such as Yes-associated protein (YAP), leading to gene expression changes that impact processes like proliferation, survival, or differentiation (Ishihara & Haga, 2022).

In melanoma cells, MAPK signaling components have recently been reported to negatively regulate MITF nuclear localization and activity in melanoma cells: RAF proteins, acting upstream of ERK, interact directly with MITF, causing its cytoplasmic retention and reduced transcriptional activity (Estrada et al., 2022), while MAPK/ERK signaling, in collaboration with GSK3, controls MITF nuclear export (Ngeow et al., 2018). The transcriptional co-activator YAP, known to translocate into the nucleus in response to ECM stiffening in various cell types (Cai et al., 2021; Dupont et al., 2011; Huang et al., 2022; Miskolczi et al., 2018), promotes MITF expression in uveal and cutaneous melanoma cells (Barbosa et al., 2023; Miskolczi et al., 2018) and serves as MITF cofactor in uveal melanoma (Barbosa et al., 2023). This indicates a dual role of YAP in the control of MITF in melanoma. However, whether and how ECM cues modulate MITF remains to be elucidated.

So far, studies have separately explored the roles of ECM type and substrate stiffness for MC biology. For example, Hara et al. reported that COL IV stimulates dendricity in human MCs on glass substrates (considered as ultra-hard stiffness) (Hara et al., 1994), while melanin production on stiff PDMS substrates (5.5 MPa) coated with laminin is higher compared to softer counterparts (from 50 kPa to 1.8 MPa) (Choi et al., 2014). However, the potential synergistic effects of substrate stiffness and ECM components on MC functions remain to be defined. Understanding such effects is particularly important since the ECM undergoes continuous remodeling that includes de novo synthesis and degradation (Pfisterer et al., 2021). Various factors, such as skin aging, inflammation, sunlight exposure, wound healing, and fibrosis, can promote ECM remodeling, potentially resulting in aberrant ECM modifications (Pfisterer et al.,

2021), which may modify the presentation of ECM ligands and alter substrate stiffness. Nevertheless, it is still insufficiently understood how substrate stiffness influences the cellular responses to specific ECM components, and, conversely, whether cells need to engage in particular ECM interactions in order to sense environmental stiffness features.

This study investigated whether and how substrate stiffness and ECM components synergize to modulate MC functions. We compared the combined effects of various ECM proteins and substrate stiffness on MC behavior. Our results revealed that ECM components control MC differentiation and function via an ERK-MITF axis, with different ECM types determining the ability of MCs to perceive and respond to mechanical stimuli in their environment.

## *RESULTS*

### *ECM components differentially affect MC morphology, adhesion and migration*

To assess how extracellular mechanical cues affect MC behavior, we employed PDMS substrates of varying stiffnesses: ≈45 kPa defined here as soft, ≈140 kPa as intermediate and ≈1 MPa 900 kPa as stiff (fig. S1). This range was chosen to reflect the wide range of stiffness found within the skin and because increased environmental stiffness is associated with multiple pathologies (Diazzi et al., 2020; Pfisterer et al., 2021; Wang et al., 2023). To mimic both normal and altered ECM conditions, COL IV-, COL I-, and FN-coated substrates of varying stiffness were used for cultures of either primary (pMCs) or immortalized murine MCs (stably expressing membrane-targeted tandem dimer Tomato; iMCs, generated for this study), followed by molecular, cellular and functional assays.

Since cell spreading is regulated by coordinated changes in adhesions to ECM and cytoskeletal reorganization, we examined the cell area as well as key cell adhesion parameters. Among these, FAK activity by means of its autophosphorylation (p-FAK) and quantification of the number of focal adhesions (FAs) per cell served as indicators of responses resulting from MC-ECM interactions. In both pMCs and iMCs, the smallest cell area was detected on COL I (fig. 1A,B; fig. S2A) and correlated with the lowest p-FAK levels (fig. 1A,C; fig. S2B), whereas the largest cell areas (fig. 1A,B; fig. S2A) were found on FN, correlating with high p-FAK signals (fig. 1A,C; fig. S2B). These data delineate that COL I and FN trigger opposite MC responses. Substrate stiffness, however, seemed to have less influence on the cell area: apart from a slight increase from soft to intermediate stiffness in iMCs cultured on COL I, we did not note significant changes of the cell area across the different substrate stiffnesses, regardless of the ECM protein used (fig. 1B; fig. S2A). In contrast, both p-FAK and the number of FAs per µm² exhibited a significant stiffness-mediated increase in MCs grown on FN-coated substrates (fig. 1C,D; fig. S2B,C). The overall low p-FAK levels in on COL I-

exposed iMCs instead even decreased with stiffness (fig. 1C), highlighting that stiffness sensing in MCs depends on the ECM type.

Interestingly, visual inspection in phase-contrast and fluorescence microscopy showed that iMCs cultured on COL IV- and FN-coated substrates exhibited a more dendritic shape compared to the mostly bi- or tripolar appearing MCs grown on COL I (fig. 1A). To examine this phenotype further, we performed a Sholl analysis (fig. 1E; fig. S3A; Binley et al., 2014; Sholl, 1953). Quantification of the dendritic complexity of MCs (fig. 1F) and the corresponding Sholl profile (fig. 1G; fig. S3B) confirmed that most iMCs exposed to COL IV and FN displayed between 4 to 7 dendrites, whereas MCs grown on COL I exhibited mostly 2 to 3 dendrites (fig. 1F). Noteworthy, over the range of stiffnesses tested, MC dendricity was not impacted by substrate stiffness, irrespective of the ECM protein type used (fig. S3B). Finally, since FAs and cell morphology are closely linked to cell movement, we next investigated whether the distinct ECM molecules influence MC motility. Live cell imaging of iMCs revealed that both the distance traveled (fig. 2A-C) and velocity (fig. 2D) of cell migration decreased on COL I compared to COL IV and FN, whereas FN-grown iMCs showed increased motility (fig. 2A-C) and faster migration (fig. 2D) relative to their COL IV-grown counterparts.

Together, these data show that COL I and FN trigger opposite morphological, adhesive and migratory phenotypes in MCs.

***COL I and FN have opposite effects on melanin production and MC proliferation***

Given the observed role of ECM components for MC morphology and migration, we next investigated whether ECM cues influence other MC functions. As a hallmark task of MCs, we examined their melanin production by measuring both intracellular melanin contents and melanin released into the culture medium. iMC grown on COL I-coated substrates exhibited the highest intra- and extracellular melanin content, while melanin levels on FN were lowest compared to COL I and COL IV (fig. 3A,B). Notably, the expression of *Tyr*, an essential gene for melanogenesis, correlated with melanin production, exhibiting a higher expression in iMCs exposed to COL I than in those exposed to FN (fig. 3C). Like iMCs, pMCs cultured on FN produced least melanin on soft and intermediate stiffness (fig. S2D). For all ECM types tested, highest values for melanin production were observed at high stiffness (fig. S2D, fig. 3A,B). Collectively, these data demonstrated that compared to COL I, FN restricts melanin production.

Using a BrdU assay, we next evaluated MC proliferation. While stiffness had no effect on MC proliferation in the presence of COL IV and FN, we observed a higher proportion of BrdU-positive iMCs when exposed to stiff COL I-coated substrates, indicating a synergistic effect of COL I and stiffness on MC proliferation (fig. 3D). Among the three ECM types tested, FN

exposure resulted in lowest proliferation rates (fig. 3D), a finding that could be further confirmed by live cell imaging and subsequent analysis of the percentage of dividing cells (fig. 3E). Overall, these experiments revealed a stiffness-dependent proliferative phenotype triggered by COL I, while FN appears to restrict cell division of MCs.

Together, our findings show that melanin production and *Tyr* expression are highest in MCs exposed to COL I and lowest in FN-grown MCs. Moreover, cell proliferation was lowest on FN, and stiffness-mediated increase in proliferation was only observed on COL I-coated substrates, suggesting that MC mechanoresponses depend on the ECM type.

***MITF nuclear localization is modulated by ECM molecules and substrate stiffness but does not correlate with nuclear YAP***

Our data indicate an ECM-dependent regulation of MC proliferation and melanin production, with COL I and FN driving opposite effects on these cellular functions. Considering the central role of the transcription factor MITF in the control of both melanogenesis and cell cycle progression (Goding & Arnheiter, 2019), plus the observed increase of the MITF target gene *Tyr* on COL I (fig. 3C), we next examined the subcellular localization of MITF and its dependence on ECM cues. As observed for melanin levels, highest nuclear MITF levels were detected on COL I-coated substrates, while MCs on FN displayed low nuclear MITF levels (fig. 4A,B; fig. S2E). Furthermore, a stiffness-mediated increase of MITF nuclear localization was noted in MCs on COL I (fig. 4A,B; fig. S2E), thus identifying MITF as an ECM- and mechanosensitive transcription factor. The contrasting phenotypes of MCs grown on COL I vs. FN were also evident when correlating nuclear MITF levels to the cell area (fig. S4A): while MCs grown on COL I were characterized by a low ratio of cell area to nuclear MITF compared to COL IV, FN-exposed MCs showed high ratios, i.e. a large cell area was associated with low MITF. Interestingly, this ratio decreased with substrate stiffness on COL I and FN but not on COL IV (fig. S4A), suggesting that changes in nuclear MITF are not linearly related to morphological changes in response to ECM. Given that YAP is a transcriptional co-activator known to translocate into the nucleus in response to ECM stiffening in various cell types, including melanoma cells (Miskolczi et al., 2018), and may serve as potential MITF partner in uveal melanoma cells (Barbosa et al., 2023), we wondered whether YAP could be associated with the observed ECM-dependent MC phenotypes. We examined YAP subcellular localization and, consistent with previous reports, observed a stiffness-mediated increase in nuclear YAP, with the strongest response at intermediate stiffness levels on COL IV and COL I, and on stiff FN-coated substrates (fig. 4C,D). Importantly, however, unlike nuclear MITF, we did not observe significant differences of nuclear YAP when comparing the three ECM types, making it unlikely that MCs utilize YAP for ECM-specific melanin production.

Collectively, our findings suggest that ECM subtypes regulate MC behavior and function likely through modulation of MITF localization and activity, independently of YAP.

### ***ECM-dependent ERK activation controls MITF localization and activity, as well as melanogenesis***

After delineating ECM- and substrate stiffness-dependent MC functions, we aimed to decipher intracellular signals that link the sensing of ECM cues at the MC periphery to nuclear MITF localization and melanin production. As mentioned, the MAPK/ERK signaling pathway has been reported to be activated in response to ECM signals (Crozet & Levayer, 2023; Paszek et al., 2005; Provenzano et al., 2009). Moreover, in melanoma cells, MAPK/ERK has recently been shown to negatively control MITF nuclear localization and activity (Estrada et al., 2022; Ngeow et al., 2018). Thus, we first tested whether in iMCs, ERK is regulated in an ECM- and stiffness-dependent manner. Immunoblot analyses of ERK1/2 phosphorylation (p-ERK) indeed revealed an ECM-dependent modulation of ERK activity, with FN-grown iMCs featuring highest p-ERK levels, and COL I-exposed MCs displaying lowest p-ERK levels (fig. 5A). Moreover, iMCs cultured on COL IV or FN but not COL I showed the highest ERK activity on stiff substrates (fig. 5A), suggesting a stiffness-mediated ERK activation depending on the ECM type.

Considering these differential p-ERK signals observed with the various ECM types, we next asked whether ERK activation was causal for the observed ECM-dependent MC responses. For this, we used Trametinib, a pharmacological inhibitor targeting MEK, the upstream kinase mediating ERK phosphorylation and activation (Gilmartin et al., 2011). Intriguingly, next to the expected loss of ERK phosphorylation (fig. 5B), treatment with Trametinib resulted in an increase in nuclear MITF in iMCs exposed to COL IV and FN, reaching the nuclear MITF levels observed on COL I (fig. 5C). This indicates that ERK activity in MCs negatively regulates nuclear MITF levels. Congruent with this, Trametinib treatment increased *Tyr* mRNA expression (fig. 5D) as well as melanin production (fig. 5E) by iMCs cultured on both COL IV- and FN-coated substrates towards those levels observed in COL I conditions. Together, these data demonstrate that FN-mediated ERK activation counteracts MITF nuclear accumulation and melanin synthesis, suggesting that MEK/ERK act as negative regulators of melanogenesis in response to ECM cues.

In summary, we deciphered that distinct ECM proteins in the MC environment steer melanogenesis through differential activation of the MEK/ERK pathway and subsequent regulation of MITF localization and activity. We further showed that COL I and FN exert opposite effects on MC behavior and functions: COL I elicits a highly pigmented and proliferative, but non-motile MC state, while FN triggers a less pigmented, low proliferative and

highly motile MC state. Finally, by combining varying substrate stiffness and distinct ECM types we delineated that stiffness-mediated MC functions rely on specific ECM components.

## *DISCUSSION*

### *ECM components elicit phenotypic shifts in MCs*

Our study highlights the pivotal role of ECM components in regulating MC behavior and their adaptation to environmental cues. Specifically, we observed that compared to the physiological matrix environment of epidermal MCs (COL IV), COL I and FN – representative of a dermal matrix and thus an altered environment – elicit notable phenotypic shifts in MCs. COL I triggers melanin production but limits MC migration, whereas a FN-rich environment rewires MCs towards a slow-cycling, motile and dedifferentiated phenotype, characterized by lower melanin production and proliferation but higher migration capabilities. These findings underscore the importance of ECM composition for MC function and differentiation, with relevance not only for MC homeostasis but potentially also for pathophysiological states and stress responses.

Our data open the possibility that ECM alterations can disrupt MC homeostasis, which could have both beneficial and detrimental consequences for skin health. For instance, wound healing reflects a complex physiological process in which MC phenotypic shifts could have a significant impact. The initial stage entails the formation of a provisional FN-rich environment (Potekaev et al., 2021), which may facilitate the repopulation of MCs within the regenerated tissue (Snell, 1963). This, together with our observation of increased MC motility on FN-coated substrates (fig. 2), suggests that a FN-rich environment is beneficial for the migratory capacity of MCs in tissue repair.

Contrary, in vitiligo, the loss of epidermal MCs – resulting in characteristic non-pigmented patches – is associated with a decrease in COL IV and FN and a concomitant increase in COL I content (Rani et al., 2023). The repigmentation process requires MCs to migrate into depigmented areas and synthesize melanin effectively (Norris et al., 1994). Considering our observation of strongly reduced MC migration on COL I, it seems plausible that COL I enrichment in vitiligo lesions interferes with the efficient MC redistribution into depigmented areas in the skin. Furthermore, melasma is a multifactorial skin condition that is characterized by focal hypermelanosis. Sex hormones and UV radiation have been implicated in the development of melasma (Espósito et al., 2022). Interestingly, disruption of the basement membrane has also been reported in 96% of melasma lesions, with MCs protruding into the dermal layer in 66% of cases (Torres-Álvarez et al., 2011). While the mechanism of this dermal invasion by MCs remains open, it has been proposed that the migration of “hyperactive” MCs into the dermis leads to the constant hyperpigmentation in melasma (Phansuk et al., 2022; Torres-Álvarez et al., 2011). This concept would be in line with our findings of COL I-triggered

melanogenesis, opening the possibility that MC hyperactivity in melasma could at least in part be caused by the exposure to dermal COL I.

Finally, the dedifferentiated phenotype observed in FN-exposed MCs is reminiscent of the phenotypic changes occurring in malignant transformation of MCs. Indeed, in a mouse model recapitulating features of human melanomagenesis, it has been shown that mature MCs expressing a B-Raf oncogene can undergo transcriptional reprogramming, associated with a loss of their differentiated characteristics and eventually invasion into the dermis (Köhler et al., 2017). This suggests that MC dedifferentiation precedes MC transformation and melanoma development. Hence, the dedifferentiated phenotype observed in FN-exposed MCs could reflect one of several steps that are required during early stages of melanoma initiation. Taken together, this raises the possibility that a FN-rich environment, combined with oncogenic mutations, could render MCs susceptible to transformation and ultimately melanomagenesis.

In conclusion, our findings underscore the plasticity of MCs and their ability to switch between phenotypic states in response to environmental cues, highlighting the importance of ECM molecules in regulating MC behavior. Understanding how different conditions elicit these shifts could provide valuable insights into normal skin physiology, the mechanisms underlying melanocyte-related conditions like melanoma, and potential therapeutic targets for restoring normal melanocyte function in pigmentation disorders.

***ECM-dependent ERK activation controls MITF localization and activity, and melanogenesis***

Our findings demonstrate that ECM-dependent phenotypic shifts of MCs are linked to differential activation of the MEK/ERK pathway, and that such control of ERK activity determines the localization and output of MITF. Specifically, COL I limits ERK activity, triggering high nuclear MITF, while FN stimulates high ERK activity resulting in reduced nuclear MITF levels. This is further associated with adaptation of MC functions under the control of MITF, whereby proliferation and melanin production are enhanced on COL I but reduced on FN. In line with previous studies that linked RAF and MEK/ERK activation to cytoplasmic retention and nuclear export of MITF in melanoma cells, respectively (Estrada et al., 2022; Ngeow et al., 2018), we here demonstrate in MCs that MEK inhibition reverted the low nuclear MITF and melanin production in FN-exposed MCs. This, together with our findings on ECM-dependent differential ERK activation in MCs, identifies a hitherto unrecognized role of ECM cues in MITF nuclear localization through the regulation of ERK activity.

Nonetheless, at present, the signaling molecules transducing ECM sensing to activation of ERK remain elusive. Given the noticeable correlation between elevated FAK and ERK activity in FN-exposed MCs and considering that FAK has been reported to transduce ECM signals

through MAPK/ERK (Paszek et al., 2005), FAK appeared to be an interesting candidate for modulating p-ERK levels in MCs. However, treatment of MCs with the FAK inhibitor Defactinib did not result in the expected reduction in p-ERK levels that would align with such model (data not shown). We cannot formally rule out that Defactinib treatment in our system led to bypass mechanisms, such as receptor tyrosine kinases like EGFR directly phosphorylating the FAK autophosphorylation site, as previously reported (Marlowe et al., 2016). Further investigation is needed to clarify whether FAK acts as an upstream regulator of ERK in MCs. Other possible candidates, such as the receptor tyrosine kinase cKIT, which affects MC functions and activates MAPK/ERK (Hocker et al., 2008), showed low expression in MCs cultured on FN-coated substrates compared to COL I (data not shown). Although this does not rule out that the activity of cKIT is elevated in MCs exposed to FN, such reduced expression makes it unlikely that cKIT counteracts MITF function in the system studied here. Future work is necessary to dissect the exact molecular signals downstream of FN that control the shift of mature MCs toward less differentiated characteristics.

***Interplay between ECM components and substrate stiffness in the mechanosensation of MCs***

Our findings underpin a crucial role for ECM components in regulating mechanosensation in MCs and show that ECM components and substrate stiffness synergistically govern MC functions. So far, studies have predominantly explored either the roles of different ECM subtypes using ultra-hard substrates like glass or plastic (Hara et al., 1994), or focused on the impact of substrate stiffness with a single ECM type (Choi et al., 2014). In contrast, our approach, combining varying substrate stiffness with different ECM proteins, demonstrated that 1) over the range of stiffness and ECM molecules tested, matrix protein subtypes can dominate over mechanical substrate surface properties, as altering ECM proteins produced more pronounced effects on MC behavior compared to changes in substrate stiffness; and 2) the ability of MCs to respond to mechanical cues is highly dependent on the specific ECM proteins present. Notably, COL I supports stiffness-induced MITF nuclear localization and MC proliferation, while FN enhances mechanosensitive responses at the level of FAK activation and number of FAs. Seong et al. previously reported that in a human fibrosarcoma cell line stiffness-mediated FAK activation can be observed on FN- but not on COL I-coated substrates (Seong et al., 2013). While our observations in MCs are consistent with such effects on FN, iMCs cultured on COL I even showed reduced FAK activity with substrate stiffness, and pMCs had lowest FAK activity at intermediate stiffness. These observations suggest cell type-specific roles of ECM molecules in mechanoresponses.

Strikingly, our data identified MITF as a novel ECM- and mechanosensitive transcription factor, with a stiffness-dependent increase as well as the highest nuclear localization observed on

COL I compared to COL IV and FN. Such fine-tuning of MITF subcellular localization may ensure that MC responses are appropriately matched to the environmental matrix protein composition and mechanical features of the ECM. Overall, this highlights the context-dependent nature of MITF regulation downstream of ERK, revealing a hitherto unknown aspect of MITF modulation by ECM cues. Furthermore, our findings suggest that ECM components and substrate stiffness do not merely exert additive effects; instead, individual ECM types demonstrate synergistic interactions with stiffness in regulating MC behavior. This underscores the importance of considering both ECM protein composition and mechanical properties in future studies, as the interplay between these factors significantly influences how cells interpret and respond to mechanical signals, thereby affecting cellular function and differentiation pathways.

### *Conclusion*

In summary, we report a novel ECM-dependent MEK/ERK/MITF axis that controls the plasticity of MCs in response to interactions with their environment. Our findings underscore the critical role of the ECM in orchestrating MC function and differentiation, highlighting the need for further studies to fully understand the intricate crosstalk between mechanical parameters and ECM ligands in the cellular microenvironment (fig. 6). Moreover, our data point to a complex link between ECM protein types and substrate stiffness, which can synergistically influence MC mechanosensation (fig. 6). Elucidating the specific molecular mechanisms driving this interplay, particularly the roles of MITF and other key regulators, will be crucial for a comprehensive understanding of MC function and pathology.

## *METHODS*

### *Preparation of PDMS substrates with tunable stiffness and ECM protein coating*

Polydimethylsiloxane (PDMS) substrates were prepared using a SYLGARD 184 Elastomer kit (Dow Silicones, USA) and varying the crosslinker:silicone base agent ratio to 1:60, 1:35, and 1:10, respectively (Fig. S1). Once mixed, the PDMS elastomers were cured at 60°C for 16 h. To enhance the hydrophilicity of the substrates and facilitate binding of ECM proteins, all substrates underwent argon plasma treatment using a PDC-002-CE plasma cleaner (Harrick Plasma, USA) at 300 mTorr for 2 min. The substrates were then coated for 2 h at 37°C with 30 µg/ml of mouse collagen IV (Cultrex™, #3410-010-02, Bio-Techne, Germany), 30 µg/ml of type I collagen from calf skin (Collagen G, L7213, Sigma-Aldrich, USA), or 10 µg/ml of bovine plasma fibronectin (F1141, Sigma-Aldrich, USA) diluted in sterile D-PBS (Gibco, USA). After incubation, the excess ECM solution was aspirated, and substrates were washed with sterile D-PBS prior to cell seeding.

***Determination of the elastic modulus of uncoated and coated PDMS surfaces***

Atomic Force Microscopy (AFM) served to determine the elastic modulus (Young's Modulus) of uncoated and protein-coated PDMS surfaces used in this study. For this, the PDMS elastomers (ratio 1:10, 1:35 or 1:60) were prepared in an AFM-suitable imaging dish (ibiTreat µ-Dish, Ibidi, Germany) and transferred to the sample stage of the microscope (Nanowizard 4, Bruker Nano GmbH, Germany). An AFM cantilever with a spherical tip (Biosphere B2000, Nanotools, Germany) with a nominal spring constant of 0.2 N/m and a sphere radius of 2 µm was used to perform nanoindentation measurements. AFM force-distance measurements were conducted in a grid of 4 x 4 points with a lateral distance of 4 µm (= one tip diameter) between two points to probe native spots. The AFM cantilever was extended to the PDMS surface with a speed of 1 µm/s and pressed on it with a loading force of 20 nN. Afterwards, the cantilever was retracted with 1 µm/s to complete the force-distance measurements. For each force-distance curve, the Hertz fit (Horvath et al., 2019) was applied to the contact region of the extend curve to evaluate the Young's Modulus with the JPK SPM Data Processing Software v8.0.1 (Bruker Nano GmbH, Germany).

***Mice***

All mice were housed and maintained according to federal guidelines within the specific pathogen free (SPF) animal facility in Building 61.4 of the Saarland University in Homburg under the breeding license of Sandra Iden's lab (§11 Az. 2.4.1.1- Iden). All experiments were performed in line with German animal welfare laws as well as institutional guidelines and were reported to the responsible authorities (Vorabmeldung VM2023-16 and previous notifications). Wildtype (wt) mice were either purchased from the Jackson Laboratory (Charles River Germany) or were taken from in-house breedings of transgenic mouse lines. In those cases, F1 and F2 generation were genotyped to verify the wt alleles of the genes of interest of the respective mouse line.

***Isolation and culture of primary mouse melanocytes***

Primary mouse MCs were isolated from the epidermis of newborn wt mice and maintained up to passage 3 as previously described (Mescher et al., 2017). Briefly, to separate epidermis from dermis, whole skin from mice at postnatal day (P)0-P3 were incubated in a solution of 5 mg/ml Dispase II (Sigma-Aldrich, Germany) diluted in RPMI medium (Gibco, USA) supplemented with 10% fetal calf serum (FCS, Sigma Aldrich, Germany), penicillin (100 U/ml), streptomycin (100 µg/ml), 100 nM sodium pyruvate, and 10 mM non-essential amino acids (all Gibco, USA) at 4°C overnight. The next day, the epidermis was incubated for 20 min in TrypLE select (Gibco, USA) at room temperature. Dissociated cells were collected and cultured in RPMI medium containing 200 nM TPA (12-O-tetradecanoylphorbol-13-acetate, Sigma-Aldrich, Germany, #P8139) and 200 pM cholera toxin (Sigma-Aldrich, Germany, #C8052), hereafter

referred to as RPMI+. At passage 0, the cell cultures contained non pigmented melanoblasts, MCs, and keratinocytes. After 7 days, cells were passaged, and due to terminal differentiation, keratinocytes were largely removed, resulting in MC monocultures suitable for further experiments.

***Generation of stable murine melanocyte cell lines (iMCs)***

Immortalized MCs (iMCs) were generated by immortalizing mouse primary MCs (mTmG-positive) with SV40 large T antigen, followed by subcloning. The cells express membrane-targeted tandem dimer Tomato (dt; Muzumdar et al., 2007), yielding red fluorescence. iMCs exhibit morphological and molecular characteristics common to normal murine skin MCs. iMCs were maintained in culture in RPMI+ at 37°C with 5% $CO_2$.

***Immunofluorescence***

To assess cell area and morphology, and for quantification of MITF, YAP and p-FAK signal intensities, MCs were seeded on the different substrate combinations at a density of 2,500 cells/cm², to avoid overcrowding and allow single cell measurements. 24 h later, MCs were fixed in 4% PFA/PBS for 10 min and blocked for 1 h at room temperature with 5% bovine serum albumin (BSA) in TBS containing 0.2% Triton X-100 (named blocking buffer hereafter). Primary antibody incubation was performed in blocking buffer diluted at a ratio of 1:5 in TBS at 4°C overnight, and after 3x washing in 0.2% Tween/TBS, MCs were stained with AlexaFluor-conjugated secondary antibodies, DAPI (Carl Roth, Germany) and phalloidin to stain actin for pMCs for 1 h at room temperature. After washing, PDMS scaffolds were mounted onto glass coverslips using Fluoromount-G™ (#00-4958-02, Thermo Fisher Scientific). Antibodies used for immunostainings are listed in the Antibodies and reagents section.

***BrdU Assay***

48 h post-plating, MCs were incubated with 160 µg/ml of BrdU (5-Brom-2′-desoxyuridin; Roche) for 2 h at 37°C and then washed with PBS and fixed with 4% PFA for 10 min at room temperature. Cells were treated with 2 N HCl for 10 min at room temperature to achieve DNA denaturation, followed by a PBS wash and subsequent immunofluorescence staining as previously described.

***Microscopy***

Epifluorescence micrographs were acquired with an AxioObserver Z1 inverted microscope equipped with a Colibri 7 LED light source (Zeiss, Germany) using a Plan-Apochromat 20x/0.8 air objective an EC Plan Neofluar 40x/1.3 oil objective, a Plan-Apochromat 63x/1.4 oil objective and an Axiocam 305 camera (Zeiss, Germany) or Rolera ECM2 camera coupled to the ZEN Blue imaging software V2.6 (Zeiss, Germany).

***Image quantification***

Image analysis was performed using Fiji/ImageJ software (Schindelin et al., 2012; Schneider et al., 2012) to quantify cell area, morphology, FAK phosphorylation and focal adhesion numbers, as well as YAP and MITF nuclear translocation in MCs 24 h post-plating.

*MC dendricity and cell area:* Epifluorescence micrographs of actin (phalloidin staining) or td-Tomato, for pMCs and iMCs respectively, were preprocessed using "mean" filter to smoothen images, by reducing noise and averaging pixel values, followed by the "median" filter, which further reduced noise while preserving edges and details. Images were then converted into binary images by using the "Threshold" function to obtain a mask of the cell shape. The binary mask was used either for cell area quantification or for the quantitative assessment of morphological characteristics of MCs. Using the "Sholl Analysis" plugin, concentric circles (named radius), were drawn on the binary image at regular intervals (5 µm) from the center of the cell body. The number of intersections between dendrites and each radius was counted and then plotted to create a Sholl profile, which shows the number of dendrite intersections at increasing distances from the cell body (Binley et al., 2014; Sholl, 1953).

*p-FAK immunoreactivity:* To quantify p-FAK immunoreactivity in MCs, actin (phalloidin staining) or td-Tomato signals were used to detect the cell contour of pMCs and iMCs, respectively. This contour was then superimposed on p-FAK signal, followed by measurement of the integrated density of the signal of individual MCs. For iMCs, data were pooled after normalization for each experiment as two different microscope cameras have been used for these experimental series.

*Focal adhesion number:* To quantify the number of focal adhesions based on p-FAK signals, first, a background subtraction was performed using a rolling ball algorithm. Then, a suitable threshold was applied to isolate the focal adhesion signal from the background. Individual focal adhesions were detected using the “analyze particles” function (0.05-5 µm). Finally, the number of focal adhesions per cell and per unit area was determined.

*YAP and MITF nuclear localization:* To evaluate YAP nuclear localization in response to ECM cues, DAPI served as nuclear counterstain to delineate nuclear contour and was overlaid onto YAP signal. Then, YAP nuclear integrated density of individual MC was collected, followed by a normalization for each experiment with iMCs due to the use of two different cameras along this experimental series. To assess MITF immunoreactivity, actin (phalloidin staining) or td-Tomato was employed to delineate cell contours for pMCs and iMCs, respectively; and DAPI served as nuclear counterstain. Subsequently, the entire cell contour and nuclear contour were overlaid onto MITF signal. The integrated density of the signal from individual MCs was then quantified within the whole cell or nuclear masks. Finally, to evaluate MITF nuclear localization

in response to ECM cues, the percentage of nuclear MITF (nuclear value/whole cell value x 100) was calculated.

*BrdU assay – cell proliferation:* Proliferating MCs were quantified from at least 20 randomly positioned micrographs. The background signal was subtracted from the measured signal of each nucleus to identify BrdU-positive cells. The proliferation rate was then determined by counting BrdU-positive cells and dividing this number by the total number of cells, identified via DAPI staining.

***Live-cell imaging for analysis of MC motility***

Live-cell imaging was conducted to investigate dynamic cellular behaviors in response to ECM. Taking advantage of the stable expression of the fluorescent membrane-targeted Tomato, MCs were seeded at a density of 1,000 cells/cm² in plastic chamber slide coated with the distinct ECM proteins (µ-Slide 8 Well, Ibidi), and placed in a live cell imaging system (Zeiss Celldiscoverer 7) equipped with a temperature- and $CO_2$-controlled chamber. Time-lapse images were acquired every 20 min for 20 h using the epifluorescence microscopy mode. Two methodologies were employed to enable real-time dynamic visualization and quantitative analysis of cell migration. To quantify migration parameters, i.e., total distance migrated by cells, and their speed, cells were tracked using the “Manual tracking” plugin in Fiji software. Additionally, the “Temporal Color Code” in Fiji software was applied to track cell shape and movement over time, allowing to visualize changes of MC dynamics over time. Briefly, different colors represent the shape and position of cells at each time point, with the color gradient indicating the progression of time. The overlay of different colors provides information on the dynamic behavior of cells throughout the observation period.

***RT-qPCR***

For quantitative RT-PCRs, RNA was isolated from MCs using TRIzol reagent according to the manufacturer’s protocol (Invitrogen#15596026, ThermoFisher Scientific). RNA was reversely transcribed using a QuantiTect Reverse Transcription kit (Qiagen) and amplified with iTaq Universal Probes Supermix (Biorad). Target gene expression was detected using TaqMan probes (GAPDH mouse Mm99999915_g1; Tyr mouse Mm00495817_m1; Tyrp2 mouse Mm01225584_m1; Thermo Fisher Scientific). Gene expression changes were calculated using the comparative CT (ΔΔCT) method, normalized to GAPDH expression, and compared to cell lysates from soft substrates coated with COL IV.

***Melanin content assay***

The melanin assay was performed to quantify the average melanin amount produced by a cell. Both intracellular melanin and extracellular melanin content (i.e., melanin released into the medium) were measured from the same batch of cells. For melanin assays, each condition

was performed in duplicate: one well was used for melanin extraction, and the other for cell counting. MCs were cultured in 12-well plates for 72 h in 1 mL phenol red-free RPMI medium (Gibco, USA) to avoid interference with extracellular melanin measurements. The medium was then collected and analyzed to measure extracellular melanin content. Intracellular melanin was quantified following an adapted protocol from Ito and Wakamatsu (Ito & Wakamatsu, 2003). MCs were lysed in 400 µL of 10% DMSO in 1 N NaOH (extraction buffer) and incubated with agitation (24 h at 100°C for pMCs and 18 h at 80°C for iMCs). Extracellular extracts were quickly centrifuged for 10 sec to sediment cellular debris, and intracellular extracts were centrifuged for 5 min at 13.000 rpm. Extra- and intracellular extracts and their respective blanks, RPMI media or lysis buffer, were loaded onto a 96-well plate and absorbance was measured at 405 nm using a Multiskan™ FC Microplate Photometer (Thermo Fisher Scientific, USA). For analysis, the OD values were subtracted by the blank to remove background signals caused by the medium or lysis buffer. Next, extracellular values were multiplied by 5 and intracellular by 2 to account for the stock volume, and the values were divided by the cell number to obtain the relative melanin content per cell.

***Preparation of cell extracts, SDS-PAGE, and immunoblotting***

MCs cultures were lysed using boiled SDS/EDTA solution (1% SDS, 10 mM EDTA) and genomic DNA was sheared by passing the lysates through a 27 G x ¾ canula. Protein concentrations were quantified using the BCA assay according to the manufacturer's protocol (Pierce, Thermo Fisher Scientific). SDS-PAGE was carried out using 8-10% polyacrylamide gels. After completing gel electrophoresis, the proteins were transferred onto a PVDF membrane at 20 V for 60 min. Following the transfer, the membrane was blocked for 1 h at room temperature using 5% BSA/TBST (TBS containing 0.2% Tween 20). The primary antibody was incubated in 5% BSA/TBST overnight at 4°C on a roller. Membranes were then washed 3x for 10 min with TBST and incubated with an HRP-conjugated secondary antibody in 5% BSA/TBST for 1 h at room temperature on a roller. Membranes were washed 3x for 10 min with TBST, excess TBST was removed, and membranes were incubated 1 min with in a 1:1 mixture of ECL solutions A and B (PerkinElmer, USA). Excess ECL solution was removed, and the membrane was imaged using the Amersham ImageQuant™ 800 detector (Cytiva). Following a 30-min wash at room temperature with a buffer containing 0.2 M glycine and 0.1% SDS (pH 2.5) to strip the membranes, they were blocked and immunoblotted for total ERK using the same membranes previously used for phospho-ERK detection.

***Quantification of phospho-ERK signal in immunoblot analyses***

The protein band intensity of non-saturated Western blot signals was quantified using Fiji software. Each band was selected on the original .tiff image obtained with the Amersham ImageQuant™ 800 Detector, and the "Plot Lanes" tool generated intensity profiles. Peaks

corresponding to individual bands (related to total or phosphorylated protein) were identified, and the area under them was measured. The p-ERK/total ERK ratio was calculated to assess relative ERK activity under the different conditions. The values were normalized to the sum of each membrane's values to determine the mean and standard deviation across experiments.

***Inhibitor treatment***

To assess the role of ERK activity for ECM-dependent MC functions, MCs were seeded 4 h prior a 24h- or 72h-treatment with 100 nM Trametinib (MEK inhibitor, Biozol, #10999) diluted in RPMI+.

***Antibodies***

Details on antibodies and dyes used in this study are listed in the following Table S1.

***Statistical analyses***

Statistical analysis was performed using GraphPad Prism software (GraphPad, version 10.2.1). Measures of pooled data, from at least three independent experiments, are represented by mean and SD or SEM, as indicated in the figure legends. All data sets were subjected to normality tests (Anderson-Darling test, D'Agostino & Pearson test, Kolmogorov-Smirnov test, or Shapiro-Wilk test) when applicable. Then, statistical significance was determined using One-way ANOVA with Welch's correction (unequal variances) with Dunnett's T3 post-hoc test; RM one-way ANOVA with Geisser-Greenhouse's correction (unequal variances) with Tukey's post-hoc test; Ordinary two-way ANOVA Tukey's post-hoc test; Multiple t tests with the Holm-Sidak method's correction with Dunn's post-hoc test; and for non-Gaussian datasets using Kruskal-Wallis test with Dunn's post-hoc test, as indicated in the figure legends. P-values are ranged as follows: *, $P < 0.05$; **, $P < 0.01$; ***, $P < 0.001$; and ****, $P < 0.0001$, as detailed in the Table S2. The number of independent biological replicates and number of single cells analyzed is specified in each figure legend and in the Table S2.

***Software***

Data collection used the following software: Microscopy: ZEN Blue 2.6 (Zeiss); Immunoblot: Amersham ImageQuant™ 800 control software (Cytiva); qRT-PCR: CFX Opus 96 (BioRad). For data analysis, the following softwares were used: GraphPad PRISM, version 10.2.1, ImageJ/Fiji, JPK SPM Data Processing Software v8.0.1 (Bruker, Nano, Germany).

***ACKNOWLEDGEMENTS***

We thank the animal facility of the Faculty of Medicine, Saarland University, for important services, and the Department of Cellular Neurophysiology (CIPMM, Saarland University) for kindly providing access to the plasma cleaner. We further thank all members of the Iden laboratory for stimulating discussions.

## *CONFLICT OF INTEREST*

The authors declare no competing interests.


## *FUNDING*

This project was funded by the Deutsche Forschungsgemeinschaft (DFG, German Research Foundation) Projektnummer 200049484, SFB 1027 (projects A12 to S.I. and B2 to M.B.) and DFG INST 256/583-1 FUGG.


## *DATA AVAILABILITY*

Correspondence and requests for materials related to this study should be sent to carole.luthold@uni-saarland.de and sandra.iden@uks.eu. All data supporting the findings of this study are available within the paper and its supplemental information, or from the corresponding author on reasonable request.

## *AUTHOR CONTRIBUTIONS*

Conceptualization, Methodology, Validation, and Supervision: C.L., S.I.; Investigation: C.L., M.D., E.B., N.D., G.G., V.S.R., A.K.B., A.R.; Formal analysis: C.L., M.D., E.B., G.G., V.S.R., S.I.; Resources: M.B., S.I.; Visualization and Writing - original draft: C.L.; Writing - review and editing: C.L., S.I.; and Funding acquisition: S.I.

## *REFERENCES*


Amano, S. (2009). Possible Involvement of Basement Membrane Damage in Skin Photoaging. *Journal of Investigative Dermatology Symposium Proceedings*, *14*(1), 2–7. https://doi.org/10.1038/jidsymp.2009.5

Amano, S. (2016). Characterization and mechanisms of photoageing-related changes in skin. Damages of basement membrane and dermal structures. *Experimental Dermatology*, *25*(S3), 14–19. https://doi.org/10.1111/exd.13085

Arozarena, I., & Wellbrock, C. (2019). Phenotype plasticity as enabler of melanoma progression and therapy resistance. *Nature Reviews Cancer*, *19*(7), 377–391. https://doi.org/10.1038/s41568-019-0154-4

Barbosa, I. A. M., Gopalakrishnan, R., Mercan, S., Mourikis, T. P., Martin, T., Wengert, S., Sheng, C., Ji, F., Lopes, R., Knehr, J., Altorfer, M., Lindeman, A., Russ, C., Naumann, U., Golji, J., Sprouffske, K., Barys, L., Tordella, L., Schübeler, D., … Galli, G. G. (2023). Cancer lineage-specific regulation of YAP responsive elements revealed through large-scale functional epigenomic screens. *Nature Communications*, *14*(1), 3907. https://doi.org/10.1038/s41467-023-39527-w

Benito-Martínez, S., Salavessa, L., Raposo, G., Marks, M. S., & Delevoye, C. (2021). Melanin Transfer and Fate within Keratinocytes in Human Skin Pigmentation. *Integrative and Comparative Biology*, *61*(4), 1546–1555. https://doi.org/10.1093/icb/icab094

Biggs, L. C., Kim, C. S., Miroshnikova, Y. A., & Wickström, S. A. (2020). Mechanical Forces in the Skin: Roles in Tissue Architecture, Stability, and Function. *Journal of Investigative Dermatology*, *140*(2), 284–290. https://doi.org/10.1016/j.jid.2019.06.137

Binley, K. E., Ng, W. S., Tribble, J. R., Song, B., & Morgan, J. E. (2014). Sholl analysis: A quantitative comparison of semi-automated methods. *Journal of Neuroscience Methods*, *225*, 65–70. https://doi.org/10.1016/j.jneumeth.2014.01.017

Bonnans, C., Chou, J., & Werb, Z. (2014). Remodelling the extracellular matrix in development and disease. *Nature Reviews. Molecular Cell Biology*, *15*(12), 786–801. https://doi.org/10.1038/nrm3904

Cai, X., Wang, K.-C., & Meng, Z. (2021). Mechanoregulation of YAP and TAZ in Cellular Homeostasis and Disease Progression. *Frontiers in Cell and Developmental Biology*, *9*. https://doi.org/10.3389/fcell.2021.673599

Carreira, S., Goodall, J., Denat, L., Rodriguez, M., Nuciforo, P., Hoek, K. S., Testori, A., Larue, L., & Goding, C. R. (2006). Mitf regulation of Dia1 controls melanoma proliferation and invasiveness. *Genes & Development*, *20*(24), 3426–3439. https://doi.org/10.1101/gad.406406

Centeno, P. P., Pavet, V., & Marais, R. (2023). The journey from melanocytes to melanoma. *Nature Reviews Cancer*, *23*(6), 372–390. https://doi.org/10.1038/s41568-023-00565-7

Cheli, Y., Giuliano, S., Botton, T., Rocchi, S., Hofman, V., Hofman, P., Bahadoran, P., Bertolotto, C., & Ballotti, R. (2011). Mitf is the key molecular switch between mouse or human melanoma initiating cells and their differentiated progeny. *Oncogene*, *30*(20), 2307–2318. https://doi.org/10.1038/onc.2010.598

Choi, H., Kim, M., Ahn, S. I., Cho, E.-G., Lee, T. R., & Shin, J. H. (2014). Regulation of pigmentation by substrate elasticity in normal human melanocytes and melanotic MNT1 human melanoma cells. *Experimental Dermatology*, *23*(3), 172–177. https://doi.org/10.1111/exd.12343

Coutant, K., Magne, B., Ferland, K., Fuentes-Rodriguez, A., Chancy, O., Mitchell, A., Germain, L., & Landreville, S. (2024). Melanocytes in regenerative medicine applications and disease modeling. *Journal of Translational Medicine*, *22*(1), 336. https://doi.org/10.1186/s12967-024-05113-x

Crozet, F., & Levayer, R. (2023). Emerging roles and mechanisms of ERK pathway mechanosensing. *Cellular and Molecular Life Sciences: CMLS*, *80*(12), 355. https://doi.org/10.1007/s00018-023-05007-z

Cui, Y.-Z., & Man, X.-Y. (2023). Biology of melanocytes in mammals. *Frontiers in Cell and Developmental Biology*, *11*, 1309557. https://doi.org/10.3389/fcell.2023.1309557

Diazzi, S., Tartare-Deckert, S., & Deckert, M. (2020). Bad Neighborhood: Fibrotic Stroma as a New Player in Melanoma Resistance to Targeted Therapies. *Cancers*, *12*(6), 1364. https://doi.org/10.3390/cancers12061364

Domingues, L., Hurbain, I., Gilles-Marsens, F., Sirés-Campos, J., André, N., Dewulf, M., Romao, M., Viaris de Lesegno, C., Macé, A.-S., Blouin, C., Guéré, C., Vié, K., Raposo, G., Lamaze, C., & Delevoye, C. (2020). Coupling of melanocyte signaling and mechanics by caveolae is required for human skin pigmentation. *Nature Communications*, *11*(1), 2988. https://doi.org/10.1038/s41467-020-16738-z

Dupont, S., Morsut, L., Aragona, M., Enzo, E., Giulitti, S., Cordenonsi, M., Zanconato, F., Digabel, J. L., Forcato, M., Bicciato, S., Elvassore, N., & Piccolo, S. (2011). Role of YAP/TAZ in mechanotransduction. *Nature*, *474*(7350), 179–183. https://doi.org/10.1038/nature10137

Ebrahimighaei, R., Tarassova, N., Bond, S. C., McNeill, M. C., Hathway, T., Vohra, H., Newby, A. C., & Bond, M. (2024). Extracellular matrix stiffness controls cardiac fibroblast proliferation via the nuclear factor-Y (NF-Y) transcription factor. *Biochimica et Biophysica Acta (BBA) - Molecular Cell Research*, *1871*(2), 119640. https://doi.org/10.1016/j.bbamcr.2023.119640

Espósito, A. C. C., Cassiano, D. P., da Silva, C. N., Lima, P. B., Dias, J. A. F., Hassun, K., Bagatin, E., Miot, L. D. B., & Miot, H. A. (2022). Update on Melasma-Part I: Pathogenesis. *Dermatology and Therapy*, *12*(9), 1967–1988. https://doi.org/10.1007/s13555-022-00779-x

Estrada, C., Mirabal-Ortega, L., Méry, L., Dingli, F., Besse, L., Messaoudi, C., Loew, D., Pouponnot, C., Bertolotto, C., Eychène, A., & Druillennec, S. (2022). MITF activity is regulated by a direct interaction with RAF proteins in melanoma cells. *Communications Biology*, *5*(1), Article 1. https://doi.org/10.1038/s42003-022-03049-w

Feng, X., Li, G.-Y., Ramier, A., Eltony, A. M., & Yun, S.-H. (2022). In vivo stiffness measurement of epidermis, dermis, and hypodermis using broadband Rayleigh-wave optical coherence elastography. *Acta Biomaterialia*. https://doi.org/10.1016/j.actbio.2022.04.030

Fisher, G., & Rittié, L. (2018). Restoration of the basement membrane after wounding: A hallmark of young human skin altered with aging. *Journal of Cell Communication and Signaling*, *12*(1), 401–411. https://doi.org/10.1007/s12079-017-0417-3

Gilmartin, A. G., Bleam, M. R., Groy, A., Moss, K. G., Minthorn, E. A., Kulkarni, S. G., Rominger, C. M., Erskine, S., Fisher, K. E., Yang, J., Zappacosta, F., Annan, R., Sutton, D., & Laquerre, S. G. (2011). GSK1120212 (JTP-74057) Is an Inhibitor of MEK Activity and Activation with Favorable Pharmacokinetic Properties for Sustained In Vivo Pathway Inhibition. *Clinical Cancer Research*, *17*(5), 989–1000. https://doi.org/10.1158/1078-0432.CCR-10-2200

Goding, C. R., & Arnheiter, H. (2019). MITF—the first 25 years. *Genes & Development*, *33*(15–16), 983–1007. https://doi.org/10.1101/gad.324657.119

Graham, H. K., McConnell, J. C., Limbert, G., & Sherratt, M. J. (2019). How stiff is skin? *Experimental Dermatology*, *28 Suppl 1*, 4–9. https://doi.org/10.1111/exd.13826

Guilak, F., Cohen, D. M., Estes, B. T., Gimble, J. M., Liedtke, W., & Chen, C. S. (2009). Control of stem cell fate by physical interactions with the extracellular matrix. *Cell Stem Cell*, *5*(1), 17–26. https://doi.org/10.1016/j.stem.2009.06.016

Hara, M., Yaar, M., Tang, A., Eller, M. S., Reenstra, W., & Gilchrest, B. A. (1994). Role of integrins in melanocyte attachment and dendricity. *Journal of Cell Science*, *107*(10), 2739–2748. https://doi.org/10.1242/jcs.107.10.2739

Hirobe, T. (2014). Keratinocytes regulate the function of melanocytes. *Dermatologica Sinica*, *32*(4), 200–204. https://doi.org/10.1016/j.dsi.2014.05.002

Hocker, T. L., Singh, M. K., & Tsao, H. (2008). Melanoma Genetics and Therapeutic Approaches in the 21st Century: Moving from the Benchside to the Bedside. *Journal of Investigative Dermatology*, *128*(11), 2575–2595. https://doi.org/10.1038/jid.2008.226

Hoek, K. S., Eichhoff, O. M., Schlegel, N. C., Döbbeling, U., Kobert, N., Schaerer, L., Hemmi, S., & Dummer, R. (2008). In vivo switching of human melanoma cells between proliferative and invasive states. *Cancer Research*, *68*(3), 650–656. https://doi.org/10.1158/0008-5472.CAN-07-2491

Horvath, A. N., Holenstein, C. N., Silvan, U., & Snedeker, J. G. (2019). The Protein Mat(ters)-Revealing the Biologically Relevant Mechanical Contribution of Collagen- and Fibronectin-Coated Micropatterns. *ACS Applied Materials & Interfaces*, *11*(44), 41791–41798. https://doi.org/10.1021/acsami.9b12430

Huang, Y., Su, J., Liu, J., Yi, X., Zhou, F., Zhang, J., Wang, J., Meng, X., Si, L., & Wu, C. (2022). YAP Activation in Promoting Negative Durotaxis and Acral Melanoma Progression. *Cells*, *11*(22), 3543. https://doi.org/10.3390/cells11223543

Iriyama, S., Matsunaga, Y., Takahashi, K., Matsuzaki, K., Kumagai, N., & Amano, S. (2011). Activation of heparanase by ultraviolet B irradiation leads to functional loss of basement membrane at the dermal–epidermal junction in human skin. *Archives of Dermatological Research*, *303*(4), 253–261. https://doi.org/10.1007/s00403-010-1117-5

Iriyama, S., Yasuda, M., Nishikawa, S., Takai, E., Hosoi, J., & Amano, S. (2020). Decrease of laminin-511 in the basement membrane due to photoaging reduces epidermal stem/progenitor cells. *Scientific Reports*, *10*(1), 12592. https://doi.org/10.1038/s41598-020-69558-y

Ishihara, S., & Haga, H. (2022). Matrix Stiffness Contributes to Cancer Progression by Regulating Transcription Factors. *Cancers*, *14*(4), 1049. https://doi.org/10.3390/cancers14041049

Ito, S., & Wakamatsu, K. (2003). Quantitative Analysis of Eumelanin and Pheomelanin in Humans, Mice, and Other Animals: A Comparative Review. *Pigment Cell Research*, *16*(5), 523–531. https://doi.org/10.1034/j.1600-0749.2003.00072.x

Kawakami, A., & Fisher, D. E. (2017). The master role of microphthalmia-associated transcription factor in melanocyte and melanoma biology. *Laboratory Investigation*, *97*(6), Article 6. https://doi.org/10.1038/labinvest.2017.9

Köhler, C., Nittner, D., Rambow, F., Radaelli, E., Stanchi, F., Vandamme, N., Baggiolini, A., Sommer, L., Berx, G., van den Oord, J. J., Gerhardt, H., Blanpain, C., & Marine, J.-C. (2017). Mouse Cutaneous Melanoma Induced by Mutant BRaf Arises from Expansion and Dedifferentiation of Mature Pigmented Melanocytes. *Cell Stem Cell*, *21*(5), 679-693.e6. https://doi.org/10.1016/j.stem.2017.08.003

Marlowe, T. A., Lenzo, F. L., Figel, S. A., Grapes, A. T., & Cance, W. G. (2016). Oncogenic Receptor Tyrosine Kinases Directly Phosphorylate Focal Adhesion Kinase (FAK) as a Resistance Mechanism to FAK-Kinase Inhibitors. *Molecular Cancer Therapeutics*, *15*(12), 3028–3039. https://doi.org/10.1158/1535-7163.MCT-16-0366

Matthews, N. H., Li, W.-Q., Qureshi, A. A., Weinstock, M. A., & Cho, E. (2017). Epidemiology of Melanoma. In W. H. Ward & J. M. Farma (Eds.), *Cutaneous Melanoma: Etiology and Therapy*. Codon Publications. http://www.ncbi.nlm.nih.gov/books/NBK481862/

Mescher, M., Jeong, P., Knapp, S. K., Rübsam, M., Saynisch, M., Kranen, M., Landsberg, J., Schlaak, M., Mauch, C., Tüting, T., Niessen, C. M., & Iden, S. (2017). The epidermal polarity protein Par3 is a non–cell autonomous suppressor of malignant melanoma. *Journal of Experimental Medicine*, *214*(2), 339–358. https://doi.org/10.1084/jem.20160596

Miskolczi, Z., Smith, M. P., Rowling, E. J., Ferguson, J., Barriuso, J., & Wellbrock, C. (2018). Collagen abundance controls melanoma phenotypes through lineage-specific microenvironment sensing. *Oncogene*, *37*(23), 3166–3182. https://doi.org/10.1038/s41388-018-0209-0

Müller, J., Krijgsman, O., Tsoi, J., Robert, L., Hugo, W., Song, C., Kong, X., Possik, P. A., Cornelissen-Steijger, P. D. M., Geukes Foppen, M. H., Kemper, K., Goding, C. R., McDermott, U., Blank, C., Haanen, J., Graeber, T. G., Ribas, A., Lo, R. S., & Peeper, D. S. (2014). Low MITF/AXL ratio predicts early resistance to multiple targeted drugs in melanoma. *Nature Communications*, *5*, 5712. https://doi.org/10.1038/ncomms6712

Muzumdar, M. D., Tasic, B., Miyamichi, K., Li, L., & Luo, L. (2007). A global double-fluorescent Cre reporter mouse. *Genesis (New York, N.Y.: 2000)*, *45*(9), 593–605. https://doi.org/10.1002/dvg.20335

Ngeow, K. C., Friedrichsen, H. J., Li, L., Zeng, Z., Andrews, S., Volpon, L., Brunsdon, H., Berridge, G., Picaud, S., Fischer, R., Lisle, R., Knapp, S., Filippakopoulos, P., Knowles, H., Steingrímsson, E., Borden, K. L. B., Patton, E. E., & Goding, C. R. (2018). BRAF/MAPK and GSK3 signaling converges to control MITF nuclear export. *Proceedings of the National Academy of Sciences*, *115*(37), E8668–E8677. https://doi.org/10.1073/pnas.1810498115

Norris, D. A., Horikawa, T., & Morelli, J. G. (1994). Melanocyte Destruction and Repopulation in Vitiligo. *Pigment Cell Research*, *7*(4), 193–203. https://doi.org/10.1111/j.1600-0749.1994.tb00049.x

Paszek, M. J., Zahir, N., Johnson, K. R., Lakins, J. N., Rozenberg, G. I., Gefen, A., Reinhart-King, C. A., Margulies, S. S., Dembo, M., Boettiger, D., Hammer, D. A., & Weaver, V. M. (2005). Tensional homeostasis and the malignant phenotype. *Cancer Cell*, *8*(3), 241–254. https://doi.org/10.1016/j.ccr.2005.08.010

Pfisterer, K., Shaw, L. E., Symmank, D., & Weninger, W. (2021). The Extracellular Matrix in Skin Inflammation and Infection. *Frontiers in Cell and Developmental Biology*, *9*. https://www.frontiersin.org/article/10.3389/fcell.2021.682414

Phansuk, K., Vachiramon, V., Jurairattanaporn, N., Chanprapaph, K., & Rattananukrom, T. (2022). Dermal Pathology in Melasma: An Update Review. *Clinical, Cosmetic and Investigational Dermatology*, *15*, 11–19. https://doi.org/10.2147/CCID.S343332

Popovic, A., & Tartare-Deckert, S. (2022). Role of extracellular matrix architecture and signaling in melanoma therapeutic resistance. *Frontiers in Oncology*, *12*. https://www.frontiersin.org/articles/10.3389/fonc.2022.924553

Potekaev, N. N., Borzykh, O. B., Medvedev, G. V., Pushkin, D. V., Petrova, M. M., Petrov, A. V., Dmitrenko, D. V., Karpova, E. I., Demina, O. M., & Shnayder, N. A. (2021). The Role of Extracellular Matrix in Skin Wound Healing. *Journal of Clinical Medicine*, *10*(24), 5947. https://doi.org/10.3390/jcm10245947

Prospéri, M.-T., Giordano, C., Gomez-Duro, M., Hurbain, I., Macé, A.-S., Raposo, G., & D'Angelo, G. (2024). Extracellular vesicles released by keratinocytes regulate melanosome maturation, melanocyte dendricity, and pigment transfer. *Proceedings of the National Academy of Sciences of the United States of America*, *121*(16), e2321323121. https://doi.org/10.1073/pnas.2321323121

Provenzano, P. P., Inman, D. R., Eliceiri, K. W., & Keely, P. J. (2009). Matrix density-induced mechanoregulation of breast cell phenotype, signaling and gene expression through a FAK-ERK linkage. *Oncogene*, *28*(49), 4326–4343. https://doi.org/10.1038/onc.2009.299

Rambow, F., Marine, J.-C., & Goding, C. R. (2019). Melanoma plasticity and phenotypic diversity: Therapeutic barriers and opportunities. *Genes & Development*, *33*(19–20), 1295–1318. https://doi.org/10.1101/gad.329771.119

Rani, S., Pervaiz, N., Parsad, D., & Kumar, R. (2023). Differential expression of extracellular matrix proteins in the lesional skin of vitiligo patients. *Archives of Dermatological Research*. https://doi.org/10.1007/s00403-023-02628-z

Schindelin, J., Arganda-Carreras, I., Frise, E., Kaynig, V., Longair, M., Pietzsch, T., Preibisch, S., Rueden, C., Saalfeld, S., Schmid, B., Tinevez, J.-Y., White, D. J., Hartenstein, V., Eliceiri, K., Tomancak, P., & Cardona, A. (2012). Fiji: An open-source platform for biological-image analysis. *Nature Methods*, *9*(7), 676–682. https://doi.org/10.1038/nmeth.2019

Schneider, C. A., Rasband, W. S., & Eliceiri, K. W. (2012). NIH Image to ImageJ: 25 years of image analysis. *Nature Methods*, *9*(7), 671–675. https://doi.org/10.1038/nmeth.2089

Seong, J., Tajik, A., Sun, J., Guan, J.-L., Humphries, M. J., Craig, S. E., Shekaran, A., García, A. J., Lu, S., Lin, M. Z., Wang, N., & Wang, Y. (2013). Distinct biophysical mechanisms of focal adhesion kinase mechanoactivation by different extracellular matrix proteins. *Proceedings of the National Academy of Sciences of the United States of America*, *110*(48), 19372–19377. https://doi.org/10.1073/pnas.1307405110

Sholl, D. A. (1953). Dendritic organization in the neurons of the visual and motor cortices of the cat. *Journal of Anatomy*, *87*(4), 387–406.

Snell, R. S. (1963). A study of the melanocytes and melanin in a healing deep wound. *Journal of Anatomy*, *97*(Pt 2), 243–253.

Tan, X., Yan, Y., Song, B., Zhu, S., Mei, Q., & Wu, K. (2023). Focal adhesion kinase: From biological functions to therapeutic strategies. *Experimental Hematology & Oncology*, *12*(1), 83. https://doi.org/10.1186/s40164-023-00446-7

Tirosh, I., Izar, B., Prakadan, S. M., Wadsworth, M. H., Treacy, D., Trombetta, J. J., Rotem, A., Rodman, C., Lian, C., Murphy, G., Fallahi-Sichani, M., Dutton-Regester, K., Lin, J.-R., Cohen, O., Shah, P., Lu, D., Genshaft, A. S., Hughes, T. K., Ziegler, C. G. K., … Garraway, L. A. (2016). Dissecting the multicellular ecosystem of metastatic melanoma by single-cell RNA-seq. *Science (New York, N.Y.)*, *352*(6282), 189–196. https://doi.org/10.1126/science.aad0501

Torres-Álvarez, B., Mesa-Garza, I. G., Castanedo-Cázares, J. P., Fuentes-Ahumada, C., Oros-Ovalle, C., Navarrete-Solis, J., & Moncada, B. (2011). Histochemical and immunohistochemical study in melasma: Evidence of damage in the basal membrane. *The American Journal of Dermatopathology*, *33*(3), 291–295. https://doi.org/10.1097/DAD.0b013e3181ef2d45

Tsoi, J., Robert, L., Paraiso, K., Galvan, C., Sheu, K. M., Lay, J., Wong, D. J. L., Atefi, M., Shirazi, R., Wang, X., Braas, D., Grasso, C. S., Palaskas, N., Ribas, A., & Graeber, T. G. (2018). Multi-stage differentiation defines melanoma subtypes with differential vulnerability to drug-induced iron-dependent oxidative stress. *Cancer Cell*, *33*(5), 890-904.e5. https://doi.org/10.1016/j.ccell.2018.03.017

Walma, D. A. C., & Yamada, K. M. (2020). The extracellular matrix in development. *Development*, *147*(10), dev175596. https://doi.org/10.1242/dev.175596

Wang, K., Wen, D., Xu, X., Zhao, R., Jiang, F., Yuan, S., Zhang, Y., Gao, Y., & Li, Q. (2023). Extracellular matrix stiffness-The central cue for skin fibrosis. *Frontiers in Molecular Biosciences*, *10*, 1132353. https://doi.org/10.3389/fmolb.2023.1132353

Wouters, J., Kalender-Atak, Z., Minnoye, L., Spanier, K. I., De Waegeneer, M., Bravo González-Blas, C., Mauduit, D., Davie, K., Hulselmans, G., Najem, A., Dewaele, M., Pedri, D., Rambow, F., Makhzami, S., Christiaens, V., Ceyssens, F., Ghanem, G., Marine, J.-C., Poovathingal, S., & Aerts, S. (2020). Robust gene expression programs underlie recurrent cell states and phenotype switching in melanoma. *Nature Cell Biology*, *22*(8), 986–998. https://doi.org/10.1038/s41556-020-0547-3

Yoshihisa, Y., Norisugi, O., Matsunaga, K., Nishihira, J., & Shimizu, T. (2014). Involvement of MIF in basement membrane damage in chronically UVB-exposed skin in mice. *PloS One*, *9*(2), e89569. https://doi.org/10.1371/journal.pone.0089569

## *FIGURE LEGENDS*

**Figure 1: ECM components determine the morphology and adhesion of immortalized melanocytes.** iMCs were cultured overnight on substrates of varying stiffness defined here as soft (PDMS ratio 1:60 ≈40kPa), intermediate (PDMS ratio 1:35 ≈130kPa) and stiff (PDMS ratio 1:10 ≈1MPa) coated with COL IV, COL I or FN. **A.** Representative micrographs of iMCs (expressing membrane-targeted tandem dimer (td) Tomato) cultured on stiff substrates coated with COL IV, COL I or FN and immunostained for p-Y397-FAK and with DAPI; scale bar: 20µm. **B.** Quantification of the cell area of iMCs; violin plots display the medians and distributions of cell area in each condition; N=3, n(cells)≥69; Kruskal–Wallis test: ****: p<0.0001; **: p<0.005; *: p<0.05. **C.** Quantification of p-FAK levels; violin plots show the medians and distributions of the integrated density of p-FAK per cell; N≥4, n(cells)≥82; Kruskal–Wallis test: ****: p<0.0001; ***: p<0.001; *: p<0.05. **D.** Quantification of the number of focal adhesions per $\mu m^2$ per cell with violin plots displaying medians and distributions; N≥3, n(cells)≥65; Kruskal–Wallis test: ****: p<0.0001; *: p<0.05. **E.** Representative binary image of cells used for Sholl analysis, with radius drawn every 5µm. **F.** Quantification of the number of dendrites of iMCs; graph indicating the percentage of cells exhibiting 2 or 3 dendrites, between 4 and 7, or more than 7 dendrites; mean±SEM, N=3, n(cells)≥85. **G.** Graphs showing the Sholl profile analysis, plotting the number of dendrite intersections against the distance from the cell body. The SEM are represented by the connecting curve (dotted line); N=3, n(cells)≥85. Each curve represents an ECM type, and each graph represents a substrate stiffness condition; Welch ANOVA test: **: p<0.005; *: p<0.05. Abbreviations: A.U., arbitrary units.

**Figure 2: Differential effects of ECM proteins on iMC motility, with COL I decreasing and FN increasing motility. A.** Image showing the temporal color code analysis from live-cell imaging of iMCs cultured overnight in plastic chamber coated with COL IV, COL I or FN to visualize cell dynamics over time. The different colors represent morphology and position

of the iMCs at a given time (20min intervals), with the color gradient indicating time progression (from 0 to 240min); scale bar: 50µm. **B**. Tracks showing the path and distance of cells (one cell = one track) relative to the point of origin (time point zero) in the x and y plane. **C**. Quantification of total distance traveled by iMCs; violin plots show the medians and distributions; N=3, n(cells)≥113; Kruskal–Wallis test: ****: p<0.0001; *: p<0.05. **D**. Quantification of mean speed of iMCs; violin plots show the medians and distributions N=3, n(cells)≥113; Kruskal–Wallis test: ****: p<0.0001.

**Figure 3: COL I stimulates melanin production, and FN counteracts iMC proliferation.** **A**. Representative example of total melanin produced by iMCs cultured 72 h on substrates of varying stiffness (soft, intermediate or stiff) coated with COL IV, COL I or FN. **B.** Quantification of intra- and extracellular melanin content by spectrophotometry at 405 nm from iMCs cultured as in (A); means±SD, N≥5; Welch ANOVA test: **: p<0.005; *: p<0.05. **C.** Quantification of *Tyr* mRNA expression of iMCs cultured overnight on substrates of varying stiffness (soft, intermediate or stiff) coated with COL IV, COL I or FN; means±SD, N=3; N=2 for COL I at intermediate stiffness; Kruskal–Wallis test: **: p<0.005; *: p<0.05. **D**. Percentage of BrdU-positive cells from iMCs cultured 48 h on substrates of varying stiffness (soft, intermediate or stiff) coated with COL IV, COL I or FN; means±SD, N≥5; ordinary two-way ANOVA: ****: p<0.0001; ***: p<0.001; **: p<0.005; *: p<0.05. **E**. Percentage of dividing cells from live-cell imaging of iMCs cultured overnight on COL IV, COL I and FN; means±SD, N=3; RM one-way ANOVA test: *: p<0.05. Abbreviations: A.U., arbitrary units.

**Figure 4: MITF nuclear localization is modulated by both ECM molecules and substrate stiffness. A.** Representative micrographs of iMCs expressing td-Tomato cultured overnight on stiff substrates coated with COL IV, COL I or FN and stained for MITF and DAPI; scale bar: 20µm. A pseudo-color intensity scale ('fire' color map) was applied to enhance visualization of MITF nuclear localization. **B**. Quantification of nuclear MITF levels; violin plots show the medians and distributions of the percentage of nuclear MITF per cell; N≥3, n(cells)≥67; Kruskal–Wallis test: ****: p<0.0001; *: p<0.05. **C**. Representative micrographs of iMCs expressing td-Tomato cultured overnight on stiff substrates coated with COL IV, COL I or FN and stained for YAP and DAPI; scale bar: 20µm. A pseudo-color intensity scale ('fire' color map) was applied to enhance visualization of YAP nuclear localization. **D**. Quantification of nuclear YAP levels; violin plots show the medians and distributions of the nuclear integrated density of YAP per cell; N=3, n(cells)≥71; Kruskal–Wallis test: ***: p<0.001; *: p<0.05. Abbreviations: A.U., arbitrary units; td-Tomato, membrane-targeted tandem dimer Tomato.

**Figure 5: ECM-mediated ERK activation regulates MITF localization and melanogenesis. A.** iMCs were cultured overnight on substrates of varying stiffness (soft, intermediate or stiff) coated with COL IV, COL I or FN. Representative Western blot and associated graph depicting the quantification of p-ERK1/2 Thr202/Tyr204 to total ERK2 ratio; means±SD; COL IV, N=2; COL I and FN, N=3. Calnexin served as loading control. **B-D.** iMCs were cultured on stiff substrates coated with COL IV, COL I or FN. 4 h post-plating, a 16-hrs treatment with DMSO or 100 nM of Trametinib (= Tram; MEK inhibitor) was commenced. **B.** Representative Western blot showing the inhibition of ERK1/2 phosphorylation with Trametinib treatment. **C**. Quantification of nuclear MITF levels following MEK inhibition; violin plots showing the medians and distributions of the integrated density of nuclear MITF per cell; N=3, n(cells)≥63; Kruskal–Wallis test: ****: p<0.0001; ***: p<0.001. **D**. Quantification of *Tyr* mRNA expression after Trametinib treatment; means±SD, N=3; multiple t tests: **: p<0.005; *: p<0.05. **E**. Quantification of intra- and extracellular melanin content by spectrophotometry at 405 nm from iMCs treated 72 h with either DMSO or 100 nM Trametinib and cultured on substrates of varying stiffness (soft, intermediate or stiff) coated with COL IV, COL I or FN; means±SD, N=3; multiple t tests: ***: p<0.001; *: p<0.05. Abbreviations: A.U., arbitrary units.

**Figure 6 (graphical abstract). Upper panel:** MC differentiation is differentially modulated by ECM components. COL I promotes a differentiated phenotype by limiting ERK activation, leading to high nuclear MITF levels, associated with increased pigmentation and proliferation but reduced motility. In contrast, FN rewires MCs towards dedifferentiation, characterized by enhanced ERK activity resulting in reduced nuclear MITF and decreased pigmentation, and associated with a slow-cycling phenotype as well as increased motility. Reducing ERK activity, through MEK inhibition, restores the differentiation of MCs exposed to FN. **Lower panel:** ECM components influence how cells interpret and respond to mechanical signals: COL I enables stiffness-mediated MITF nuclear localization and MC proliferation, while FN supports a stiffness-dependent increase in focal adhesion number and FAK activation.

**Figure S1: Validation of PDMS elasticity using Atomic Force Microscopy.** Young's modulus of PDMS substrates with varying crosslinker ratios. **A**. PDMS substrate with a crosslinker:silicone base agent ratio of 1:60; means±SD, N=3; Welch ANOVA tests: ns, p>0.05. **B**. PDMS substrate with a 1:35 ratio; means±SD, N=2 COL IV 1:35, N≥3; Welch ANOVA tests: n.s.: p>0.05. **C**. PDMS substrate with a 1:10 ratio; means±SD, N=3; Welch ANOVA tests: n.s.: p>0.05.

**Figure S2: Response of primary MCs to distinct ECM cues.** pMCs were cultured overnight on substrates of varying stiffness (soft, intermediate or stiff) coated with COL IV, COL I or

FN. **A.** Violin plots showing the medians and distributions of the cell area of pMCs; N≥5, n(cells)≥96; Kruskal–Wallis test: ****: p<0.0001. **B.** Quantification of p-FAK levels; violin plots showing the medians and distributions of the integrated density of total p-FAK per cell; N=3, n(cells)≥52; Kruskal–Wallis test: ****: p<0.0001; ***: p<0.001; **: p<0.005. **C.** Quantification of FAs; violin plots showing the medians and distributions of the number of focal adhesions per $\mu m^2$ per cell; N=3, n(cells)≥65; Kruskal–Wallis test: ****: p<0.0001; **: p<0.005; *: p<0.05. **D.** Quantification of intra- and extracellular melanin content by spectrophotometry at 405 nm from pMCs cultured 72 h on substrates of varying stiffness (soft, intermediate or stiff) coated with COL IV, COL I or FN; means±SD, N=3; multiple t tests: *: p<0.05. **E.** Quantification of nuclear MITF; violin plots showing the medians and distributions of the percentage of nuclear MITF per cell; N=3, n(cells)≥67; Kruskal–Wallis test: ****: p<0.0001; ***: p<0.001; **: p<0.005; *: p<0.05. Abbreviations: A.U., arbitrary units.

**Figure S3: Sholl profiles for iMCs exposed to different ECM molecules. A.** Representative micrographs of iMCs, expressing td-Tomato, cultured overnight on stiff substrates coated with COL IV, COL I or FN, corresponding to the examples of binary images shown in figure 1E; scale bar: 20µm. **B.** Graphs showing the Sholl profile analysis, plotting the number of dendrite intersections against the distance from the cell body. The SEM are represented by the connecting curve (dotted line); N=3, n(cells)≥85. Each curve represents a substrate stiffness condition, and each graph represents an ECM type (same cells as analyzed in fig. 1G, different plotting of the data); Welch ANOVA test: n.s.: p>0.05.

**Figure S4: Negative correlation between nuclear MITF levels and MC area. A**. The percentage of nuclear MITF, from cells analyzed in figure 4, was plotted against the cell area of the corresponding MC for all stiffnesses and ECM types tested. The bar diagram depicts the means±SEM of the ratio of cell area to percentage of nuclear MITF per cell; N=3, n(cells)≥47; Kruskal–Wallis test: ****: p<0.0001; ***: p<0.001; **: p<0.005; *: p<0.05.

Luthold et al - **Figure 1**

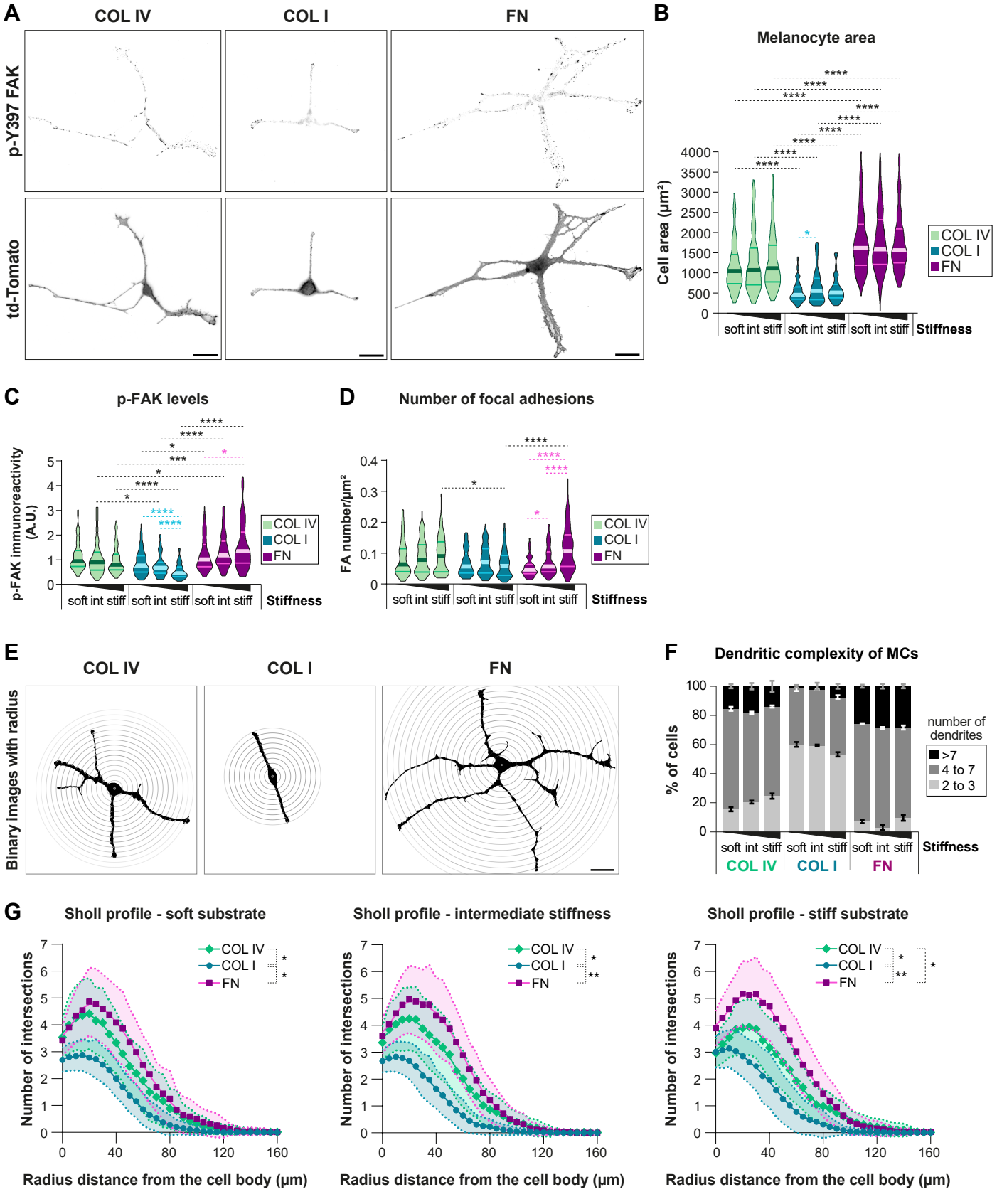

Luthold et al - **Figure 2**

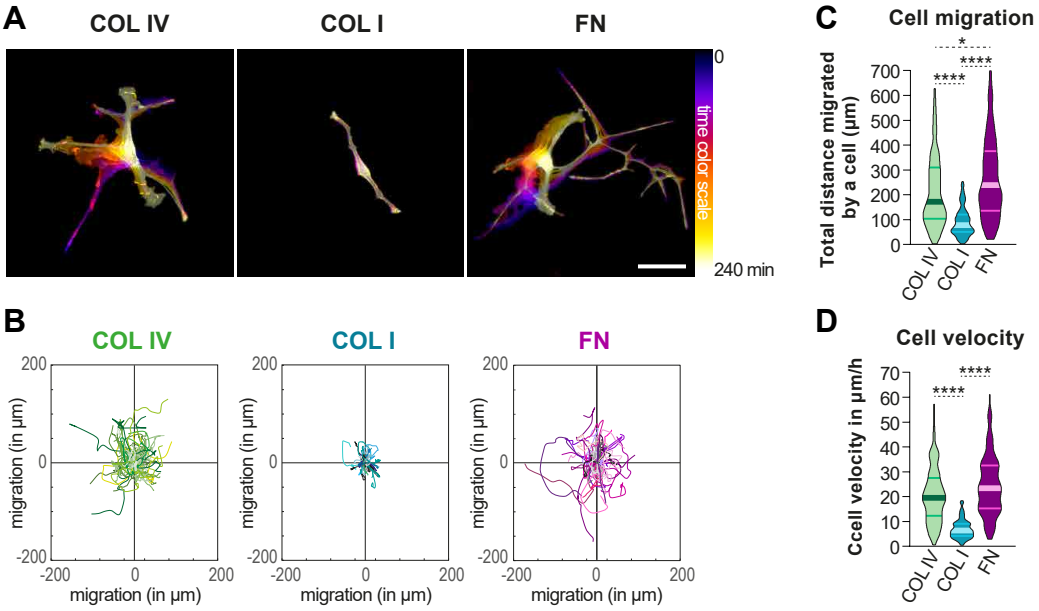

Luthold et al - **Figure 3**

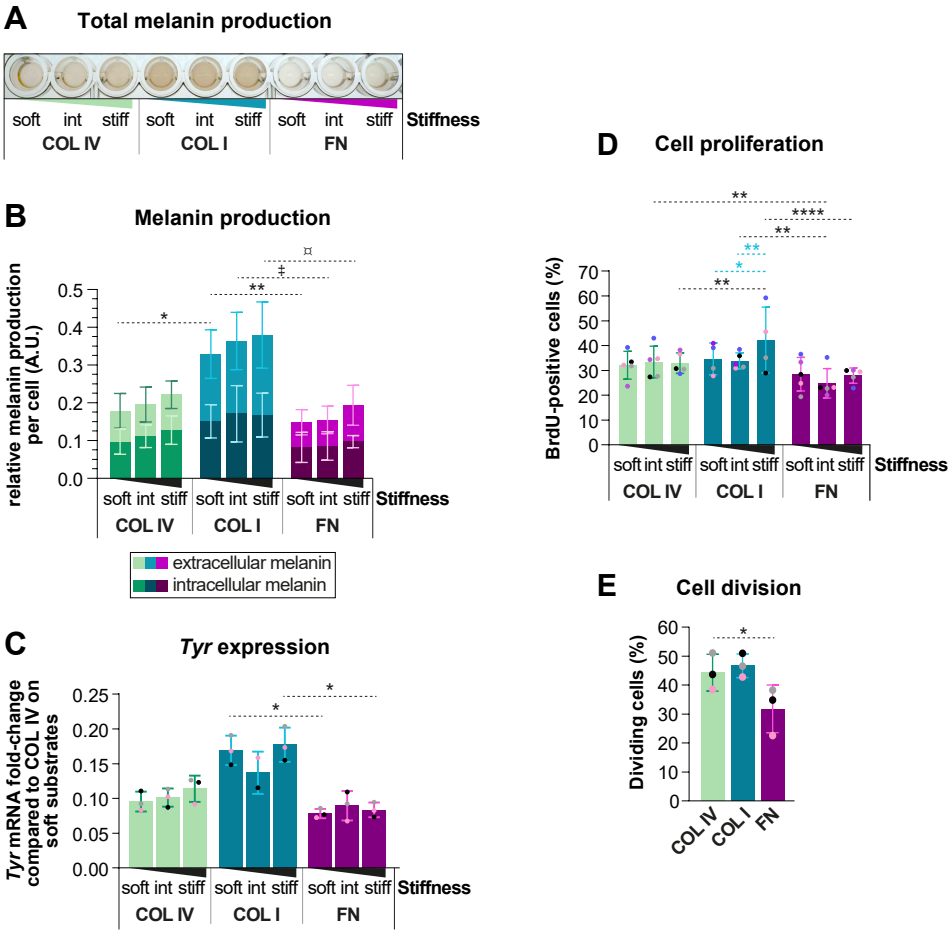

Luthold et al - **Figure 4**

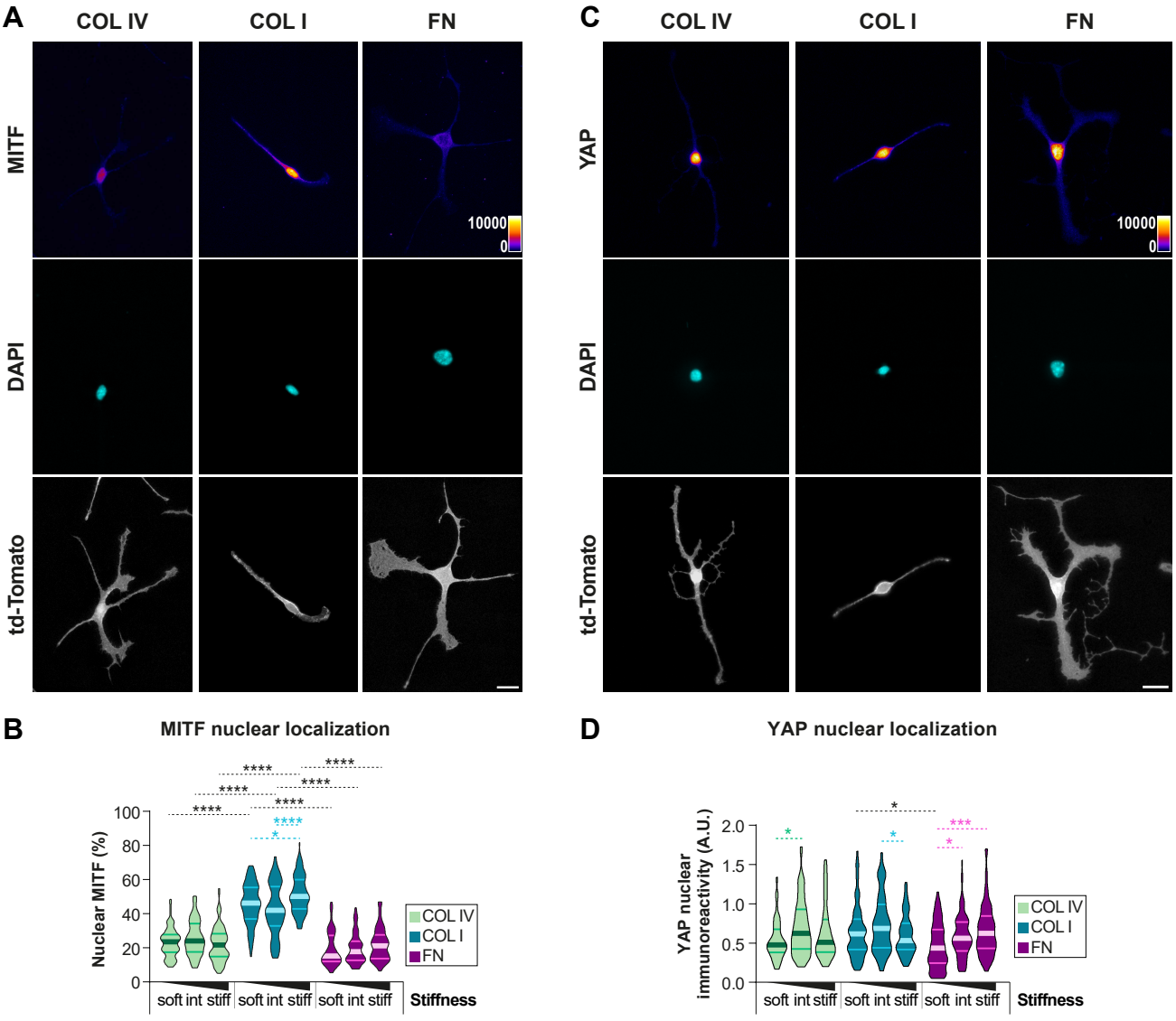

Luthold et al - **Figure 5**

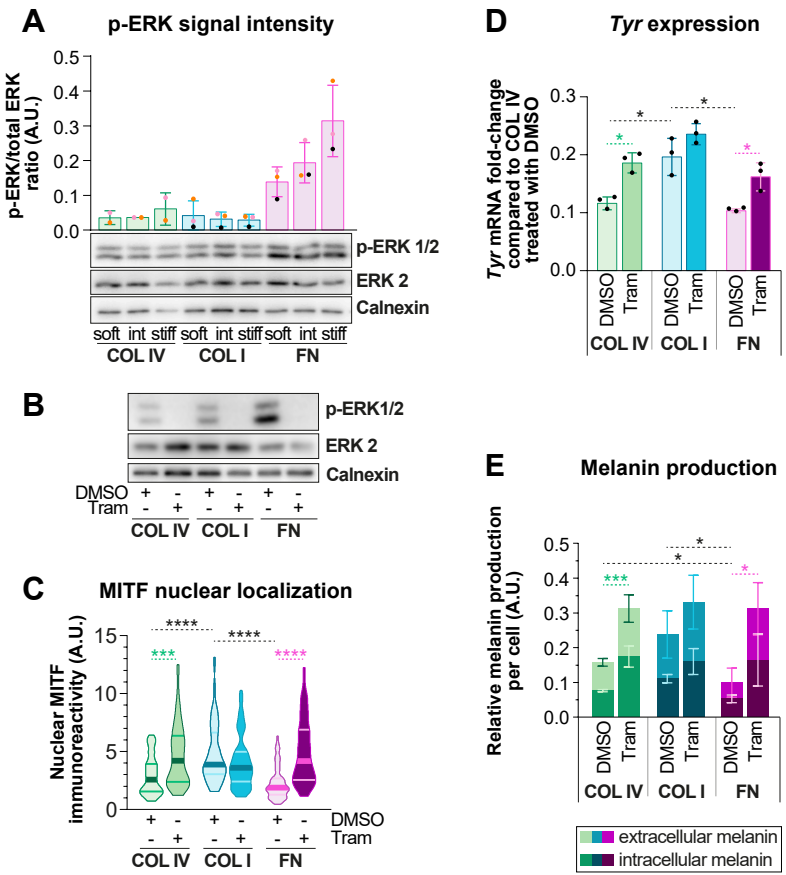

Luthold et al - **Figure 6**

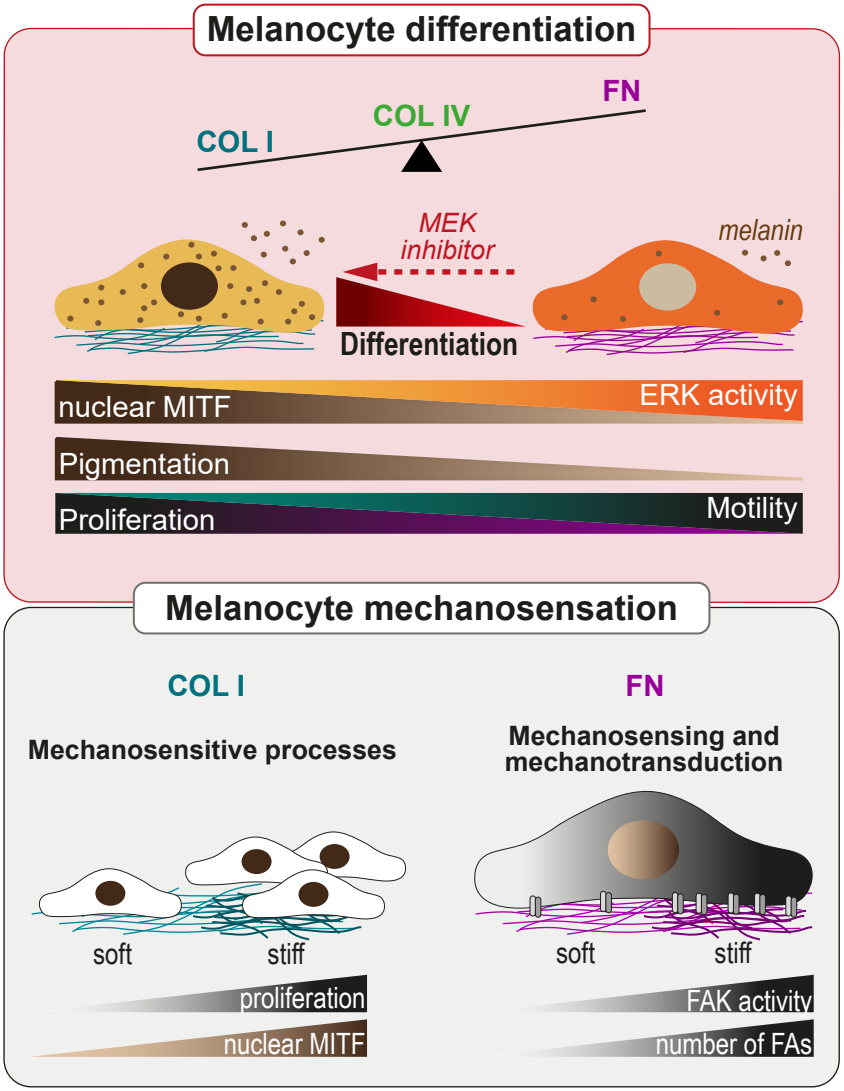

Luthold et al - **Figure S1**

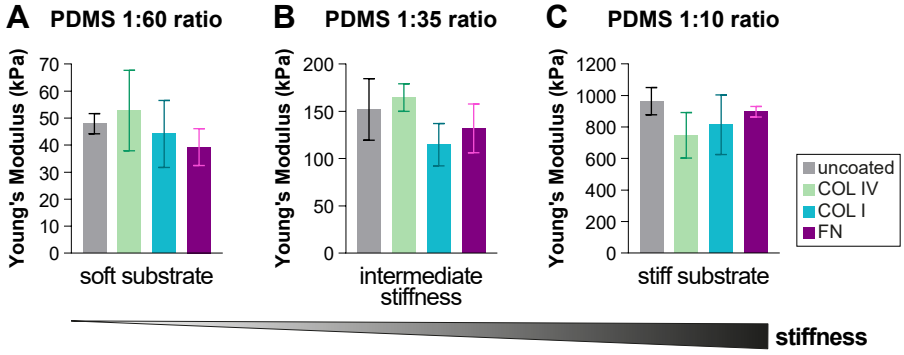

Luthold et al - **Figure S2**

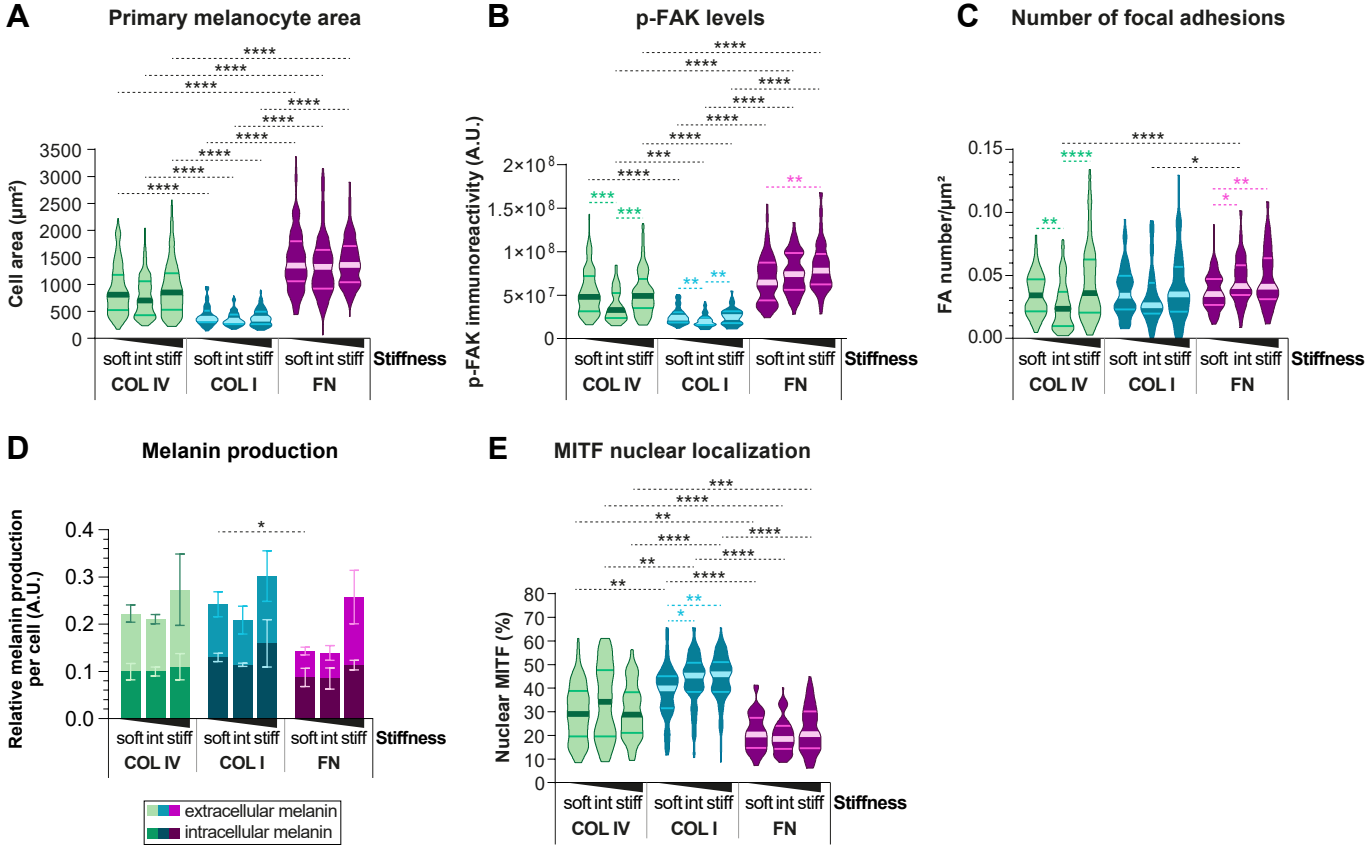

Luthold et al - **Figure S3**

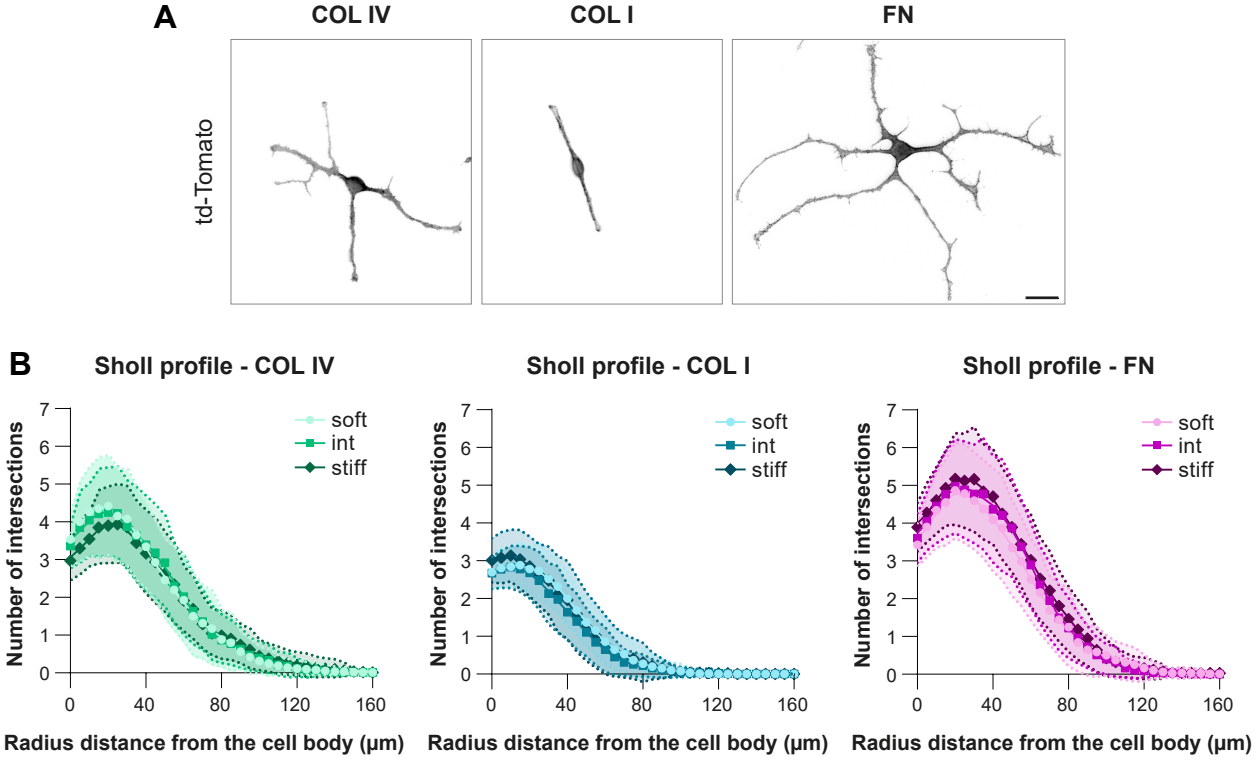

Luthold et al - **Figure S4**

**A** **Correlation between nuclear MITF and cell area**

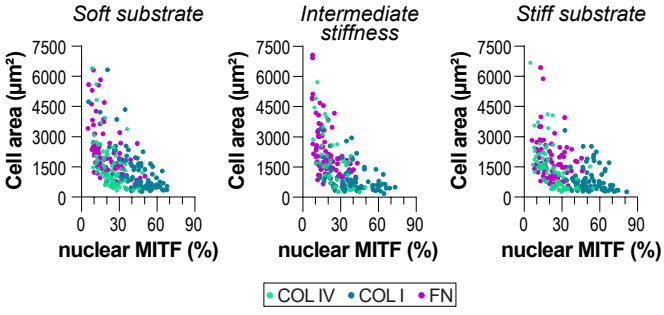


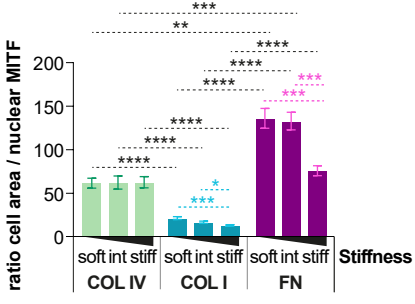

Luthold et al **Supplementary tables**

## Supplementary Table S1

| **Primary Antibodies** | | **Company** | **Catalog Nr.** |
|---|---|---|---|
| **IF** | Anti-MITF antibody [C5] | Abcam | Ab12039 |
| | Phospho-FAK (Tyr397) antibody | Cell Signaling Technology | 3283S |
| | YAP (D8H1X) XP® | Cell Signaling Technology | 14074S |
| **WB** | pERK1/2 | Cell Signaling Technology | 4370 |
| | ERK2 | BD Pharmingen | 610104 |
| | Calnexin | Enzo Life Sciences | ADI-SPA-860-D |
| **Conjugated Secondary Antibodies** | | | |
| **IF** | Alexa Fluor™ 488 donkey anti-rabbit | Invitrogen | #A-21235 |
| | Alexa Fluor™ 647 goat anti-mouse | Invitrogen | #A-21206 |
| **WB** | HRP donkey anti-rabbit | Invitrogen | A16023 |
| | HRP sheep anti-mouse | Amersham | NA931V |
| **Dyes** | | | |
| **IF** | Alexa Fluor™ 568 Phalloidin | Molecular Probes | A12380 |
| | DAPI | Carl Roth | 6335.1 |

Luthold et al - **Supplementary Table S2**

**fig 1A - cell area**

stastical test

| Pass normality test? **NO** | | | |
|---|---|---|---|
| **Kruskal-Wallis** | | | |
| **Dunn's multiple comparisons test** | | | |
| | | **Significant?** | **P Value** |
| **COL IV** | COL IV 1:60 vs. COL IV 1:35 | ns | >0,9999 |
| | COL IV 1:60 vs. COL IV 1:10 | ns | 0,8765 |
| | COL IV 1:35 vs. COL IV 1:10 | ns | >0,9999 |
| **COL I** | COL I 1:60 vs. COL I 1:35 | **** | <0,0001 |
| | COL I 1:60 vs. COL I 1:10 | ns | 0,2148 |
| | COL I 1:35 vs. COL I 1:10 | * | 0,0234 |
| **FN** | FN 1:60 vs. FN 1:35 | ns | 0,3094 |
| | FN 1:60 vs. FN 1:10 | ns | >0,9999 |
| | FN 1:35 vs. FN 1:10 | ns | 0,3022 |
| **1:60** | COL I 1:60 vs. FN 1:60 | **** | <0,0001 |
| | COL I 1:60 vs. COL IV 1:60 | **** | <0,0001 |
| | FN 1:60 vs. COL IV 1:60 | * | 0,0482 |
| **1:35** | COL I 1:35 vs. FN 1:35 | **** | <0,0001 |
| | COL I 1:35 vs. COL IV 1:35 | ** | 0,0033 |
| | FN 1:35 vs. COL IV 1:35 | ns | >0,9999 |
| **1:10** | COL I 1:10 vs. FN 1:10 | **** | <0,0001 |
| | COL I 1:10 vs. COL IV 1:10 | **** | <0,0001 |
| | FN 1:10 vs. COL IV 1:10 | ns | 0,4259 |

descriptive statistics

| | **COL IV** | | | **COL I** | | | **FN** | | |
|---|---|---|---|---|---|---|---|---|---|
| | **1:60** | **1:35** | **1:10** | **1:60** | **1:35** | **1:10** | **1:60** | **1:35** | **1:10** |
| **N exp** | 3 | | | | | | | | |
| **n cells** | 69 | 90 | 97 | 93 | 88 | 93 | 96 | 103 | 101 |
| **Mean** | 1727 | 1775 | 1950 | 804,2 | 1178 | 1027 | 2386 | 2048 | 2414 |
| SD | 993,5 | 1018 | 1187 | 507,7 | 654,7 | 736,1 | 1310 | 997,7 | 1356 |
| SEM | 119,6 | 107,3 | 120,5 | 52,64 | 69,79 | 76,33 | 133,7 | 98,3 | 134,9 |

## fig 1C - pFAK levels

stastical test

| Pass normality test? NO | | | |
|---|---|---|---|
| **Kruskal-Wallis** | | | |
| **Dunn's multiple comparisons test** | | | |
| | | **Significant?** | **P Value** |
| **COL IV** | COL IV 1:60 vs. COL IV 1:35 | ns | 0,4894 |
| | COL IV 1:60 vs. COL IV 1:10 | ns | 0,0928 |
| | COL IV 1:35 vs. COL IV 1:10 | ns | >0,9999 |
| **COL I** | COL I 1:60 vs. COL I 1:35 | ns | 0,3868 |
| | COL I 1:60 vs. COL I 1:10 | **** | <0,0001 |
| | COL I 1:35 vs. COL I 1:10 | **** | <0,0001 |
| **FN** | FN 1:60 vs. FN 1:35 | ns | 0,282 |
| | FN 1:60 vs. FN 1:10 | * | 0,0359 |
| | FN 1:35 vs. FN 1:10 | ns | 0,8607 |
| **1:60** | COL I 1:60 vs. FN 1:60 | * | 0,0256 |
| | COL I 1:60 vs. COL IV 1:60 | ns | 0,0604 |
| | FN 1:60 vs. COL IV 1:60 | ns | >0,9999 |
| **1:35** | COL I 1:35 vs. FN 1:35 | **** | <0,0001 |
| | COL I 1:35 vs. COL IV 1:35 | * | 0,0427 |
| | FN 1:35 vs. COL IV 1:35 | * | 0,0311 |
| **1:10** | COL I 1:10 vs. FN 1:10 | **** | <0,0001 |
| | COL I 1:10 vs. COL IV 1:10 | **** | <0,0001 |
| | FN 1:10 vs. COL IV 1:10 | *** | 0,0005 |

descriptive statistics

| | **COL IV** | | | **COL I** | | | **FN** | | |
|---|---|---|---|---|---|---|---|---|---|
| | **1:60** | **1:35** | **1:10** | **1:60** | **1:35** | **1:10** | **1:60** | **1:35** | **1:10** |
| **N exp** | 4 | 4 | 4 | 4 | 4 | 5 | 4 | 5 | 3 |
| **n cells** | 92 | 85 | 109 | 100 | 97 | 133 | 82 | 121 | 83 |
| **Mean** | 1,148 | 1,086 | 1,001 | 0,8877 | 0,767 | 0,5429 | 1,208 | 1,348 | 1,553 |
| SD | 0,5978 | 0,7068 | 0,5609 | 0,4956 | 0,4253 | 0,2994 | 0,6544 | 0,6813 | 0,9443 |
| SEM | 0,06233 | 0,07666 | 0,05372 | 0,04956 | 0,04319 | 0,02596 | 0,07226 | 0,06193 | 0,1037 |

## fig 1D - number of FAs

stastical test

| Pass normality test? NO | | | |
|---|---|---|---|
| **Kruskal-Wallis** | | | |
| **Dunn's multiple comparisons test** | | | |
| | | **Significant?** | **P Value** |
| **COL IV** | COL IV 1:60 vs. COL IV 1:35 | ns | >0,9999 |
| | COL IV 1:60 vs. COL IV 1:10 | ns | 0,9173 |
| | COL IV 1:35 vs. COL IV 1:10 | ns | >0,9999 |
| **COL I** | COL I 1:60 vs. COL I 1:35 | ns | >0,9999 |
| | COL I 1:60 vs. COL I 1:10 | ns | >0,9999 |
| | COL I 1:35 vs. COL I 1:10 | ns | 0,375 |
| **FN** | FN 1:60 vs. FN 1:35 | * | 0,0363 |
| | FN 1:60 vs. FN 1:10 | **** | <0,0001 |
| | FN 1:35 vs. FN 1:10 | **** | <0,0001 |
| **1:60** | COL I 1:60 vs. FN 1:60 | ns | >0,9999 |
| | COL I 1:60 vs. COL IV 1:60 | ns | >0,9999 |
| | FN 1:60 vs. COL IV 1:60 | ns | 0,0733 |
| **1:35** | COL I 1:35 vs. FN 1:35 | ns | >0,9999 |
| | COL I 1:35 vs. COL IV 1:35 | ns | >0,9999 |
| | FN 1:35 vs. COL IV 1:35 | ns | >0,9999 |
| **1:10** | COL I 1:10 vs. FN 1:10 | **** | <0,0001 |
| | COL I 1:10 vs. COL IV 1:10 | * | 0,017 |
| | FN 1:10 vs. COL IV 1:10 | ns | >0,9999 |

descriptive statistics

| | **COL IV** | | | **COL I** | | | **FN** | | |
|---|---|---|---|---|---|---|---|---|---|
| | **1:60** | **1:35** | **1:10** | **1:60** | **1:35** | **1:10** | **1:60** | **1:35** | **1:10** |
| **N exp** | 3 | 3 | 3 | 3 | 3 | 5 | 3 | 4 | 3 |
| **n cells** | 69 | 65 | 89 | 84 | 79 | 133 | 69 | 99 | 83 |
| **Mean** | 0,08505 | 0,08922 | 0,09498 | 0,06871 | 0,07679 | 0,06747 | 0,05413 | 0,0731 | 0,1162 |
| SD | 0,05818 | 0,05545 | 0,05905 | 0,04149 | 0,04721 | 0,04487 | 0,03012 | 0,04481 | 0,07241 |
| SEM | 0,007005 | 0,006878 | 0,006259 | 0,004527 | 0,005312 | 0,003891 | 0,003626 | 0,004503 | 0,007948 |

| | fig 1E - MC dendricity complexity | | | | | | | | | |
|---|---|---|---|---|---|---|---|---|---|---|
| | | COL IV | | | COL I | | | FN | | |
| | | 1:60 | 1:35 | 1:10 | 1:60 | 1:35 | 1:10 | 1:60 | 1:35 | 1:10 |
| | N exp | 3 | 3 | 3 | 3 | 3 | 3 | 3 | 3 | 3 |
| | n cells | 85 | 89 | 107 | 138 | 136 | 153 | 126 | 140 | 146 |
| mean | 2 to 3 | 15,5555556 | 20,5 | 24,6187364 | 60,0461425 | 59,359738 | 53,2537914 | 7,15242122 | 3,12178388 | 9,71516972 |
| | 4 to 7 | 68,8888889 | 61,2083333 | 61,4379085 | 38,6231082 | 38,2012376 | 39,3942329 | 67,1086278 | 68,2443539 | 61,9410319 |
| | >7 | 15,5555556 | 18,2916667 | 13,9433551 | 1,33074935 | 2,43902439 | 7,35197563 | 25,738951 | 28,6338622 | 28,3437983 |
| SEM | 2 to 3 | 1,41219758 | 1,0261342 | 1,8258221 | 1,66918658 | 0,57102161 | 1,4985177 | 1,1611834 | 1,76150372 | 2,02460515 |
| | 4 to 7 | 1,32577898 | 0,82816685 | 0,75070439 | 1,90380086 | 0,22108701 | 1,18338293 | 0,29768777 | 0,64682354 | 1,4000745 |
| | >7 | 1,41219758 | 2,19464868 | 3,77926573 | 0,84755901 | 2,43902439 | 1,69692285 | 1,00441296 | 1,61600055 | 1,42235041 |

## fig 1D - sholl profiles

stastical test

| Pass normality test? **YES** | | | |
|---|---|---|---|
| **Welch ANOVA tests** | | | |
| **Dunnett's T3 multiple comparisons test** | | | |
| | | **Significant?** | **P Value** |
| **1:60** | COL I 1:60 vs. FN 1:60 | * | 0,0101 |
| | COL I 1:60 vs. COL IV 1:60 | * | 0,024 |
| | FN 1:60 vs. COL IV 1:60 | ns | 0,3119 |
| **1:35** | COL I 1:35 vs. FN 1:35 | ** | 0,0057 |
| | COL I 1:35 vs. COL IV 1:35 | * | 0,0142 |
| | FN 1:35 vs. COL IV 1:35 | ns | 0,1536 |
| **1:10** | COL I 1:10 vs. FN 1:10 | ** | 0,0019 |
| | COL I 1:10 vs. COL IV 1:10 | * | 0,0138 |
| | FN 1:10 vs. COL IV 1:10 | * | 0,0362 |

descriptive statistics

| | **COL IV** | | | **COL I** | | | **FN** | | |
|---|---|---|---|---|---|---|---|---|---|
| | **1:60** | **1:35** | **1:10** | **1:60** | **1:35** | **1:10** | **1:60** | **1:35** | **1:10** |
| **N exp** | 3 | 3 | 3 | 3 | 3 | 3 | 3 | 3 | 3 |
| **n cells** | 85 | 89 | 107 | 138 | 136 | 153 | 126 | 140 | 146 |
| **Area under the curve** | 258,2 | 259,2 | 249,3 | 148,9 | 132,1 | 149,6 | 303 | 318,5 | 340,1 |
| Std. Error | 28,97 | 27,3 | 24,41 | 14,97 | 15,55 | 20,01 | 30,29 | 29,88 | 29,15 |

## fig 2C and 2D - cell migration and velocity

stastical test - total distance migrated

| Pass normality test? **NO** | | |
|---|---|---|
| **Kruskal-Wallis** | | |
| **Dunn's multiple comparisons test** | | |
| | **Significant?** | **P Value** |
| COL I vs. FN | **** | <0,0001 |
| COL I vs. COL IV | **** | <0,0001 |
| FN vs. COL IV | * | 0,0239 |

descriptive statistics - total distance migrated

| | **COL IV** | **COL I** | **FN** |
|---|---|---|---|
| **N exp** | 3 | 3 | 3 |
| **n cells** | 179 | 158 | 113 |
| **Mean** | 214,2 | 91,46 | 267,2 |
| SD | 142,9 | 57,47 | 159,5 |
| SEM | 10,68 | 4,572 | 15,01 |

stastical test - cell velocity

| Pass normality test? **NO** | | |
|---|---|---|
| **Kruskal-Wallis** | | |
| **Dunn's multiple comparisons test** | | |
| | **Significant?** | **P Value** |
| COL I vs. FN | **** | <0,0001 |
| COL I vs. COL IV | **** | <0,0001 |
| FN vs. COL IV | ns | 0,0792 |

descriptive statistics - cell velocity

| | **COL IV** | **COL I** | **FN** |
|---|---|---|---|
| **N exp** | 3 | 3 | 3 |
| **n cells** | 181 | 152 | 114 |
| **Mean** | 20,64 | 7,06 | 24,52 |
| SD | 11,12 | 3,804 | 12,06 |
| SEM | 0,8262 | 0,3085 | 1,129 |

## fig 3B - melanin production

stastical test

| Pass normality test? **YES (Shapiro-Wilk test)** | | | |
|---|---|---|---|
| **Welch ANOVA tests** | | | |
| **Dunnett's T3 multiple comparisons test** | | | |
| | | **Significant?** | **P Value** |
| **COL IV** | COL IV 1:60 vs. COL IV 1:35 | ns | 0,9634 |
| | COL IV 1:60 vs. COL IV 1:10 | ns | 0,6945 |
| | COL IV 1:35 vs. COL IV 1:10 | ns | 0,9057 |
| **COL I** | COL I 1:60 vs. COL I 1:35 | ns | 0,9214 |
| | COL I 1:60 vs. COL I 1:10 | ns | 0,7689 |
| | COL I 1:35 vs. COL I 1:10 | ns | 0,9936 |
| **FN** | FN 1:60 vs. FN 1:35 | ns | 0,994 |
| | FN 1:60 vs. FN 1:10 | ns | 0,3219 |
| | FN 1:35 vs. FN 1:10 | ns | 0,4965 |
| **1:60** | COL I 1:60 vs. FN 1:60 | ** | 0,0033 |
| | COL I 1:60 vs. COL IV 1:60 | * | 0,0206 |
| | FN 1:60 vs. COL IV 1:60 | ns | 0,7957 |
| **1:35** | COL I 1:35 vs. FN 1:35 | * | 0,0154 |
| | COL I 1:35 vs. COL IV 1:35 | ns | 0,0517 |
| | FN 1:35 vs. COL IV 1:35 | ns | 0,6287 |
| **1:10** | COL I 1:10 vs. FN 1:10 | * | 0,0193 |
| | COL I 1:10 vs. COL IV 1:10 | ns | 0,0515 |
| | FN 1:10 vs. COL IV 1:10 | ns | 0,8636 |

descriptive statistics

| | **COL IV** | | | **COL I** | | | **FN** | | |
|---|---|---|---|---|---|---|---|---|---|
| | **1:60** | **1:35** | **1:10** | **1:60** | **1:35** | **1:10** | **1:60** | **1:35** | **1:10** |
| **N exp** | 5 | 5 | 5 | 7 | 7 | 7 | 7 | 7 | 7 |
| **Mean** | 0,1785 | 0,1959 | 0,2216 | 0,3294 | 0,3637 | 0,3796 | 0,1502 | 0,1563 | 0,1952 |
| SD | 0,06573 | 0,06492 | 0,07062 | 0,08978 | 0,1346 | 0,1231 | 0,04679 | 0,05516 | 0,05592 |
| SEM | 0,0294 | 0,02903 | 0,03158 | 0,03393 | 0,05089 | 0,04651 | 0,01768 | 0,02085 | 0,02114 |

## fig 3C - *Tyr* expression level

stastical test

| Pass normality test? **YES (Shapiro-Wilk test)** | | | |
|---|---|---|---|
| **RM one-way ANOVA** | | | |
| **Geisser-Greenhouse's multiple comparisons test** | | | |
| | | **Significant?** | **P Value** |
| **1:60** | COL 4 vs. COL 1 | ns | 0,1144 |
| | COL 4 vs. FN | ns | 0,1171 |
| | COL 1 vs. FN | * | 0,025 |
| **1:35** | COL 4 vs. COL 1 | | |
| | COL 4 vs. FN | | |
| | COL 1 vs. FN | | |
| **1:10** | COL 4 vs. COL 1 | ns | 0,07 |
| | COL 4 vs. FN | ns | 0,0631 |
| | COL 1 vs. FN | * | 0,0285 |
| **COL IV** | 1:60 COL 4 vs. 1:35 COL 4 | ns | 0,9226 |
| | 1:60 COL 4 vs. 1:10 COL 4 | ns | 0,2509 |
| | 1:35 COL 4 vs. 1:10 COL 4 | ns | 0,6626 |
| **COL I** | 1:60 COL 1 vs. 1:35 COL 1 | | |
| | 1:60 COL 1 vs. 1:10 COL 1 | | |
| | 1:35 COL 1 vs. 1:10 COL 1 | | |
| **FN** | 1:60 FN vs. 1:35 FN | ns | 0,6401 |
| | 1:60 FN vs. 1:10 FN | ns | 0,522 |
| | 1:35 FN vs. 1:10 FN | ns | 0,9208 |

descriptive statistics

| | **COL IV** | | | **COL I** | | | **FN** | | |
|---|---|---|---|---|---|---|---|---|---|
| | **1:60** | **1:35** | **1:10** | **1:60** | **1:35** | **1:10** | **1:60** | **1:35** | **1:10** |
| **N exp** | 3 | 3 | 3 | 3 | 2 | 3 | 3 | 3 | 3 |
| **Mean** | 0,09543 | 0,1011 | 0,1139 | 0,1692 | 0,137 | 0,1774 | 0,07828 | 0,0897 | 0,08363 |
| SD | 0,01423 | 0,01314 | 0,01899 | 0,02122 | 0,03057 | 0,02462 | 0,006743 | 0,02117 | 0,01057 |

## fig 3D - cell proliferation BrdU assay

stastical test

| Ordinary two-way ANOVA<br>Tukey's multiple comparisons test | | Significant? | P Value |
|---|---|---|---|
| COL IV | 1:60 vs. 1:35 | ns | 0,9984 |
| | 1:60 vs. 1:10 | ns | >0,9999 |
| | 1:35 vs. 1:10 | ns | >0,9999 |
| COL I | 1:60 vs. 1:35 | ns | >0,9999 |
| | 1:60 vs. 1:10 | * | 0,0296 |
| | 1:35 vs. 1:10 | ** | 0,0063 |
| FN | 1:60 vs. 1:35 | ns | 0,6252 |
| | 1:60 vs. 1:10 | ns | >0,9999 |
| | 1:35 vs. 1:10 | ns | 0,7993 |
| 1:60 | COL I 1:60 vs. FN 1:60 | ns | 0,0965 |
| | COL I 1:60 vs. COL IV 1:60 | ns | 0,9351 |
| | FN 1:60 vs. COL IV 1:60 | ns | 0,6423 |
| 1:35 | COL I 1:35 vs. FN 1:35 | ** | 0,0014 |
| | COL I 1:35 vs. COL IV 1:35 | ns | >0,9999 |
| | FN 1:35 vs. COL IV 1:35 | ** | 0,0025 |
| 1:10 | COL I 1:10 vs. FN 1:10 | **** | <0,0001 |
| | COL I 1:10 vs. COL IV 1:10 | ** | 0,0019 |
| | FN 1:10 vs. COL IV 1:10 | ns | 0,2238 |

descriptive statistics

| | COL IV | | | COL I | | | FN | | |
|---|---|---|---|---|---|---|---|---|---|
| | 1:60 | 1:35 | 1:10 | 1:60 | 1:35 | 1:10 | 1:60 | 1:35 | 1:10 |
| N exp | 5 | 5 | 5 | 4 | 5 | 4 | 5 | 4 | 5 |
| Mean | 32,07363538 | 33,42574755 | 32,9322937 | 34,6525624 | 33,83666838 | 42,24035308 | 28,48825262 | 24,85155655 | 27,92725714 |
| SD | 2,499603717 | 2,858143419 | 1,856631175 | 3,176031086 | 1,439126713 | 6,636137515 | 3,043714191 | 2,659492905 | 1,367577772 |

## fig 4D - cell division

Pass normality test? **YES (Shapiro-Wilk test)**

**RM one-way ANOVA**
**Tukey's multiple comparisons test**

| | Significant? | P Value |
|---|---|---|
| **COL I vs. FN** | ns | 0,0913 |
| **COL I vs. COL IV** | ns | 0,7956 |
| **FN vs. COL IV** | * | 0,0471 |

| | COL IV | COL I | FN |
|---|---|---|---|
| **N exp** | 3 | 3 | 3 |
| **n cells** | 258 | 230 | 243 |
| **Mean** | 44,31 | 46,72 | 31,82 |
| SD | 6,306 | 4,091 | 8,261 |
| SEM | 3,641 | 2,362 | 4,769 |

## fig 4B - MITF nuclear localization

Pass normality test? **NO**

**Kruskal-Wallis**
**Dunn's multiple comparisons test**

| | | Significant? | P Value |
|---|---|---|---|
| **COL IV** | COL IV 1:60 vs. COL IV 1:35 | ns | 0,618 |
| | COL IV 1:60 vs. COL IV 1:10 | ns | >0,9999 |
| | COL IV 1:35 vs. COL IV 1:10 | ns | 0,0869 |
| **COL I** | COL I 1:60 vs. COL I 1:35 | ns | 0,3959 |
| | COL I 1:60 vs. COL I 1:10 | * | 0,0119 |
| | COL I 1:35 vs. COL I 1:10 | **** | <0,0001 |
| **FN** | FN 1:60 vs. FN 1:35 | ns | >0,9999 |
| | FN 1:60 vs. FN 1:10 | ns | 0,0596 |
| | FN 1:35 vs. FN 1:10 | ns | 0,1898 |
| **1:60** | COL I 1:60 vs. FN 1:60 | **** | <0,0001 |
| | COL I 1:60 vs. COL IV 1:60 | **** | <0,0001 |
| | FN 1:60 vs. COL IV 1:60 | ns | >0,9999 |
| **1:35** | COL I 1:35 vs. FN 1:35 | **** | <0,0001 |
| | COL I 1:35 vs. COL IV 1:35 | **** | <0,0001 |
| | FN 1:35 vs. COL IV 1:35 | ns | 0,0926 |
| **1:10** | COL I 1:10 vs. FN 1:10 | **** | <0,0001 |
| | COL I 1:10 vs. COL IV 1:10 | **** | <0,0001 |
| | FN 1:10 vs. COL IV 1:10 | ns | >0,9999 |

descriptive statistics

| | COL IV | | | COL I | | | FN | | |
|---|---|---|---|---|---|---|---|---|---|
| | **1:60** | **1:35** | **1:10** | **1:60** | **1:35** | **1:10** | **1:60** | **1:35** | **1:10** |
| **N exp** | 3 | 3 | 3 | 3 | 3 | 5 | 3 | 4 | 4 |
| **n cells** | 70 | 67 | 90 | 84 | 76 | 131 | 77 | 107 | 94 |
| **Mean** | 23,08 | 25,77 | 22,22 | 45,68 | 42,1 | 51,33 | 19,26 | 19,59 | 22,04 |
| SD | 8,568 | 10,27 | 10,36 | 12,09 | 15,05 | 10,85 | 9,964 | 8,764 | 9,514 |
| SEM | 1,024 | 1,255 | 1,092 | 1,319 | 1,726 | 0,9483 | 1,135 | 0,8473 | 0,9813 |

## fig 4D - nuclear YAP

stastical test

| Pass normality test? NO | | | |
|---|---|---|---|
| **Kruskal-Wallis** | | | |
| **Dunn's multiple comparisons test** | | | |
| | | **Significant?** | **P Value** |
| **COL IV** | COL IV 1:60 vs. COL IV 1:35 | * | 0,0147 |
| | COL IV 1:60 vs. COL IV 1:10 | ns | 0,3972 |
| | COL IV 1:35 vs. COL IV 1:10 | ns | 0,4846 |
| **COL I** | COL I 1:60 vs. COL I 1:35 | ns | 0,1505 |
| | COL I 1:60 vs. COL I 1:10 | ns | >0,9999 |
| | COL I 1:35 vs. COL I 1:10 | * | 0,0485 |
| **FN** | FN 1:60 vs. FN 1:35 | * | 0,0112 |
| | FN 1:60 vs. FN 1:10 | *** | 0,0004 |
| | FN 1:35 vs. FN 1:10 | ns | 0,8248 |
| **1:60** | COL I 1:60 vs. FN 1:60 | * | 0,0198 |
| | COL I 1:60 vs. COL IV 1:60 | ns | >0,9999 |
| | FN 1:60 vs. COL IV 1:60 | ns | >0,9999 |
| **1:35** | COL I 1:35 vs. FN 1:35 | ns | 0,6123 |
| | COL I 1:35 vs. COL IV 1:35 | ns | >0,9999 |
| | FN 1:35 vs. COL IV 1:35 | ns | >0,9999 |
| **1:10** | COL I 1:10 vs. FN 1:10 | ns | >0,9999 |
| | COL I 1:10 vs. COL IV 1:10 | ns | >0,9999 |
| | FN 1:10 vs. COL IV 1:10 | ns | >0,9999 |

descriptive statistics

| | **COL IV** | | | **COL I** | | | **FN** | | |
|---|---|---|---|---|---|---|---|---|---|
| | **1:60** | **1:35** | **1:10** | **1:60** | **1:35** | **1:10** | **1:60** | **1:35** | **1:10** |
| **N exp** | 3 | 3 | 3 | 3 | 3 | 3 | 3 | 3 | 3 |
| **n cells** | 82 | 78 | 91 | 91 | 83 | 92 | 71 | 86 | 73 |
| **Mean** | 0,5423 | 0,6992 | 0,6433 | 0,6432 | 0,7406 | 0,6014 | 0,4559 | 0,5928 | 0,6631 |
| SD | 0,2521 | 0,3472 | 0,3528 | 0,3424 | 0,3623 | 0,2587 | 0,2884 | 0,2818 | 0,3257 |
| SEM | 0,02784 | 0,03932 | 0,03698 | 0,03589 | 0,03977 | 0,02698 | 0,03423 | 0,03038 | 0,03812 |

**fig 5C - MITF nuclear localization with Trametinib treatment**

| stastical test | | |
|---|---|---|
| Pass normality test? **NO** | | |
| **Kruskal-Wallis** | | |
| **Dunn's multiple comparisons test** | | |
| | **Significant?** | **P Value** |
| **COL IV DMSO vs. COL I DMSO** | ******** | <0,0001 |
| COL IV DMSO vs. FN DMSO | ns | 0,6551 |
| **COL I DMSO vs. FN DMSO** | ******** | <0,0001 |
| **COL IV DMSO vs. COL IV Tram** | ******* | 0,0001 |
| COL I DMSO vs. COL I Tram | ns | >0,9999 |
| **FN DMSO vs. FN Tram** | ******** | <0,0001 |

| | descriptive statistics | | | | | |
|---|---|---|---|---|---|---|
| | **COL IV** | | **COL I** | | **FN** | |
| | DMSO | Tram | DMSO | Tram | DMSO | Tram |
| **N exp** | 3 | 3 | 3 | 3 | 3 | 3 |
| **n cells** | 75 | 87 | 83 | 86 | 63 | 80 |
| **Mean** | 299404 | 473727 | 480857 | 412824 | 234700 | 504157 |
| SD | 165600 | 268814 | 253877 | 227062 | 143225 | 278610 |
| SEM | 19122 | 28820 | 27867 | 24485 | 18045 | 31150 |

## fig 5D - Tyr expression with Trametinib

| stastical test | | | |
|---|---|---|---|
| Pass normality test? **YES (Shapiro-Wilk test)** | | | |
| **Multiple t tests** | | | |
| **Dunn's multiple comparisons test** | | | |
| | | **Significant?** | **Adjusted P Value** |
| **COL IV vs. COL I** | **DMSO** | * | 0,02948 |
| | **Tram** | * | 0,02948 |
| **COL IV vs. FN** | **DMSO** | ns | 0,239076 |
| | **Tram** | ns | 0,24224 |
| **COL I vs. FN** | **DMSO** | * | 0,015087 |
| | **Tram** | * | 0,015087 |
| | | | |
| **DMSO vs Tram** | **COL IV** | * | 0,012357 |
| | **COL I** | ns | 0,139977 |
| | **FN** | * | 0,029362 |

| | descriptive statistics | | | | | |
|---|---|---|---|---|---|---|
| | **COL IV** | | **COL I** | | **FN** | |
| | DMSO | Tram | DMSO | Tram | DMSO | Tram |
| **N exp** | 3 | 3 | 3 | 3 | 3 | 3 |
| **Mean** | 0,1162 | 0,186 | 0,1964 | 0,2354 | 0,1037 | 0,1622 |
| SD | 0,01089 | 0,01735 | 0,03204 | 0,01816 | 0,003171 | 0,0245 |
| SEM | 0,006287 | 0,01002 | 0,0185 | 0,01048 | 0,001831 | 0,01414 |

## fig 5E - melanin production with Trametinib

| stastical test | | |
|---|---|---|
| Pass normality test? **YES (Shapiro-Wilk test)** | | |
| **Multiple t tests** | | |
| **Dunn's multiple comparisons test** | | |
| | **Significant?** | **P Value** |
| COL IV DMSO vs. COL I DMSO | ns | 0,092307 |
| **COL IV DMSO vs. FN DMSO** | * | 0,019629 |
| **COL I DMSO vs. FN DMSO** | * | 0,019109 |
| **COL IV DMSO vs. COL IV Tram** | *** | 0,000252 |
| COL I DMSO vs. COL I Tram | ns | 0,532253 |
| **FN DMSO vs. FN Tram** | * | 0,027828 |

| | descriptive statistics | | | | | |
|---|---|---|---|---|---|---|
| | **COL IV** | | **COL I** | | **FN** | |
| | DMSO | Tram | DMSO | Tram | DMSO | Tram |
| **N exp** | 3 | 3 | 3 | 3 | 3 | 3 |
| **Mean** | 0,1582 | 0,3522 | 0,2711 | 0,3278 | 0,04884 | 0,3277 |
| SD | 0,008314 | 0,02605 | 0,08836 | 0,1135 | 0,04957 | 0,1341 |
| SEM | 0,0048 | 0,01504 | 0,05102 | 0,06554 | 0,02862 | 0,07744 |

## fig S1 - PDMS's Young's modulus

stastical test

| Pass normality test? **YES** (Shapiro-Wilk test) | | | |
|---|---|---|---|
| **Welch ANOVA tests** | | | |
| **Dunnett's T3 multiple comparisons test** | | | |
| | | **Significant?** | **P Value** |
| **1:60** | uncoated vs. COL I | ns | 0,989 |
| | uncoated vs. FN | ns | 0,4616 |
| | uncoated vs. COL IV | ns | 0,9842 |
| | COL I vs. FN | ns | 0,982 |
| | COL I vs. COL IV | ns | 0,9505 |
| | FN vs. COL IV | ns | 0,6723 |
| **1:35** | uncoated vs. COL I | ns | 0,4277 |
| | uncoated vs. FN | ns | 0,9117 |
| | uncoated vs. COL IV | | |
| | COL I vs. FN | ns | 0,9035 |
| | COL I vs. COL IV | | |
| | FN vs. COL IV | | |
| **1:10** | uncoated vs. COL I | ns | 0,7579 |
| | uncoated vs. FN | ns | 0,7492 |
| | uncoated vs. COL IV | ns | 0,3624 |
| | COL I vs. FN | ns | 0,9483 |
| | COL I vs. COL IV | ns | 0,9939 |
| | FN vs. COL IV | ns | 0,5694 |

descriptive statistics

| | **uncoated** | | | **COL IV** | | | **COL I** | | | **FN** | | |
|---|---|---|---|---|---|---|---|---|---|---|---|---|
| | **1:60** | **1:35** | **1:10** | **1:60** | **1:35** | **1:10** | **1:60** | **1:35** | **1:10** | **1:60** | **1:35** | **1:10** |
| **N exp** | 3 | 4 | 3 | 3 | 2 | 3 | 3 | 4 | 3 | 3 | 3 | 3 |
| **n cells** | 47,91 | 152 | 964,2 | 52,78 | 164,6 | 748 | 44,14 | 114,8 | 815 | 39,3 | 132 | 896,6 |
| SD | 3,725 | 32,5 | 86,42 | 14,89 | 14,5 | 144,8 | 12,37 | 22,4 | 188,6 | 6,823 | 25,75 | 33,65 |

## fig S2A - pMCs cell area

stastical test

| Pass normality test? NO | | | |
|---|---|---|---|
| **Kruskal-Wallis** | | | |
| **Dunn's multiple comparisons test** | | | |
| | | **Significant?** | **P Value** |
| **COL IV** | COL IV 1:60 vs. COL IV 1:35 | ns | 0,5372 |
| | COL IV 1:60 vs. COL IV 1:10 | ns | >0,9999 |
| | COL IV 1:35 vs. COL IV 1:10 | ns | 0,1807 |
| **COL I** | COL I 1:60 vs. COL I 1:35 | ns | 0,1552 |
| | COL I 1:60 vs. COL I 1:10 | ns | 0,7629 |
| | COL I 1:35 vs. COL I 1:10 | ns | >0,9999 |
| **FN** | FN 1:60 vs. FN 1:35 | ns | 0,4268 |
| | FN 1:60 vs. FN 1:10 | ns | >0,9999 |
| | FN 1:35 vs. FN 1:10 | ns | 0,0972 |
| **1:60** | COL I 1:60 vs. FN 1:60 | **** | <0,0001 |
| | COL I 1:60 vs. COL IV 1:60 | **** | <0,0001 |
| | FN 1:60 vs. COL IV 1:60 | **** | <0,0001 |
| **1:35** | COL I 1:35 vs. FN 1:35 | **** | <0,0001 |
| | COL I 1:35 vs. COL IV 1:35 | **** | <0,0001 |
| | FN 1:35 vs. COL IV 1:35 | **** | <0,0001 |
| **1:10** | COL I 1:10 vs. FN 1:10 | **** | <0,0001 |
| | COL I 1:10 vs. COL IV 1:10 | **** | <0,0001 |
| | FN 1:10 vs. COL IV 1:10 | **** | <0,0001 |

descriptive statistics

| | **COL IV** | | | **COL I** | | | **FN** | | |
|---|---|---|---|---|---|---|---|---|---|
| | **1:60** | **1:35** | **1:10** | **1:60** | **1:35** | **1:10** | **1:60** | **1:35** | **1:10** |
| **N exp** | 5 | 6 | 6 | 5 | 6 | 6 | 6 | 6 | 6 |
| **n cells** | 152 | 126 | 166 | 96 | 142 | 161 | 169 | 142 | 188 |
| **Mean** | 905,5 | 783,5 | 935,4 | 422 | 364,9 | 389,6 | 1449 | 1363 | 1429 |
| SD | 466,5 | 382,8 | 499,4 | 189,2 | 135 | 158,5 | 574,2 | 578,8 | 474,1 |
| SEM | 37,84 | 34,11 | 38,76 | 19,31 | 11,33 | 12,49 | 44,17 | 48,57 | 34,57 |

## fig S2B - pMCs pFAK

stastical test

| Pass normality test? NO | | | |
|---|---|---|---|
| **Kruskal-Wallis** | | | |
| **Dunn's multiple comparisons test** | | | |
| | | **Significant?** | **P Value** |
| **COL IV** | COL IV 1:60 vs. COL IV 1:35 | *** | 0,0004 |
| | COL IV 1:60 vs. COL IV 1:10 | ns | >0,9999 |
| | COL IV 1:35 vs. COL IV 1:10 | *** | 0,0005 |
| **COL I** | COL I 1:60 vs. COL I 1:35 | ** | 0,002 |
| | COL I 1:60 vs. COL I 1:10 | ns | >0,9999 |
| | COL I 1:35 vs. COL I 1:10 | ** | 0,0024 |
| **FN** | FN 1:60 vs. FN 1:35 | ns | 0,3084 |
| | FN 1:60 vs. FN 1:10 | ** | 0,0035 |
| | FN 1:35 vs. FN 1:10 | ns | 0,7979 |
| **1:60** | COL I 1:60 vs. FN 1:60 | **** | <0,0001 |
| | COL I 1:60 vs. COL IV 1:60 | **** | <0,0001 |
| | FN 1:60 vs. COL IV 1:60 | ns | 0,1 |
| **1:35** | COL I 1:35 vs. FN 1:35 | **** | <0,0001 |
| | COL I 1:35 vs. COL IV 1:35 | *** | 0,0003 |
| | FN 1:35 vs. COL IV 1:35 | **** | <0,0001 |
| **1:10** | COL I 1:10 vs. FN 1:10 | **** | <0,0001 |
| | COL I 1:10 vs. COL IV 1:10 | **** | <0,0001 |
| | FN 1:10 vs. COL IV 1:10 | **** | <0,0001 |

descriptive statistics

| | **COL IV** | | | **COL I** | | | **FN** | | |
|---|---|---|---|---|---|---|---|---|---|
| | **1:60** | **1:35** | **1:10** | **1:60** | **1:35** | **1:10** | **1:60** | **1:35** | **1:10** |
| **N exp** | 3 | 3 | 3 | 3 | 3 | 3 | 3 | 3 | 3 |
| **n cells** | 83 | 56 | 94 | 61 | 60 | 94 | 88 | 52 | 99 |
| **Mean** | 53960627 | 37850823 | 53121944 | 26372614 | 20865783 | 25719541 | 68881323 | 75897376 | 83136623 |
| SD | 25959332 | 18026407 | 25987786 | 9547453 | 7649541 | 9749189 | 27956374 | 24175255 | 29375298 |
| SEM | 2849407 | 2408880 | 2680435 | 1222426 | 987552 | 1005552 | 2980159 | 3352505 | 2952329 |

## fig S2C - pMCs number of focal adhesions

stastical test

| Pass normality test? NO | | | |
|---|---|---|---|
| **Kruskal-Wallis** | | | |
| **Dunn's multiple comparisons test** | | | |
| | | **Significant?** | **P Value** |
| **COL IV** | COL IV 1:60 vs. COL IV 1:35 | ** | 0,0081 |
| | COL IV 1:60 vs. COL IV 1:10 | ns | 0,507 |
| | COL IV 1:35 vs. COL IV 1:10 | **** | <0,0001 |
| **COL I** | COL I 1:60 vs. COL I 1:35 | ns | 0,7166 |
| | COL I 1:60 vs. COL I 1:10 | ns | >0,9999 |
| | COL I 1:35 vs. COL I 1:10 | ns | 0,1991 |
| **FN** | FN 1:60 vs. FN 1:35 | * | 0,0117 |
| | FN 1:60 vs. FN 1:10 | ** | 0,0071 |
| | FN 1:35 vs. FN 1:10 | ns | >0,9999 |
| **1:60** | COL I 1:60 vs. FN 1:60 | ns | >0,9999 |
| | COL I 1:60 vs. COL IV 1:60 | ns | >0,9999 |
| | FN 1:60 vs. COL IV 1:60 | ns | >0,9999 |
| **1:35** | COL I 1:35 vs. FN 1:35 | * | 0,0167 |
| | COL I 1:35 vs. COL IV 1:35 | ns | 0,5377 |
| | FN 1:35 vs. COL IV 1:35 | **** | <0,0001 |
| **1:10** | COL I 1:10 vs. FN 1:10 | ns | >0,9999 |
| | COL I 1:10 vs. COL IV 1:10 | ns | >0,9999 |
| | FN 1:10 vs. COL IV 1:10 | ns | >0,9999 |

descriptive statistics

| | **COL IV** | | | **COL I** | | | **FN** | | |
|---|---|---|---|---|---|---|---|---|---|
| | **1:60** | **1:35** | **1:10** | **1:60** | **1:35** | **1:10** | **1:60** | **1:35** | **1:10** |
| **N exp** | 3 | 3 | 3 | 3 | 3 | 3 | 3 | 3 | 3 |
| **n cells** | 82 | 70 | 94 | 65 | 69 | 90 | 88 | 70 | 97 |
| **Mean** | 0,03502 | 0,02651 | 0,04527 | 0,03746 | 0,03459 | 0,04262 | 0,03773 | 0,04632 | 0,0479 |
| SD | 0,01668 | 0,01922 | 0,03103 | 0,02026 | 0,02325 | 0,02915 | 0,01517 | 0,01932 | 0,02315 |
| SEM | 0,001842 | 0,002298 | 0,0032 | 0,002514 | 0,002799 | 0,003073 | 0,001617 | 0,002309 | 0,002351 |

## fig S2D - pMCs melanin production

stastical test

| Pass normality test? YES (Shapiro-Wilk test) | | | |
|---|---|---|---|
| **Multiple t tests** | | | |
| **Dunn's multiple comparisons test** | | | |
| | | **Significant?** | **P Value** |
| **soft vs. Int** | COL1 | ns | 0,4947 |
| | FN | ns | 0,8479 |
| | COL4 | ns | 0,8479 |
| **soft vs. stiff** | COL1 | ns | 0,619892 |
| | FN | ns | 0,10379 |
| | COL4 | ns | 0,619892 |
| **int vs. stiff** | COL1 | ns | 0,361807 |
| | FN | ns | 0,118759 |
| | COL4 | ns | 0,361807 |
| **COL I vs. COL IV** | 1:60 | ns | 0,868243 |
| | 1:35 | ns | 0,935696 |
| | 1:10 | ns | 0,935696 |
| **COL IV vs. FN** | 1:60 | ns | 0,053003 |
| | 1:35 | ns | 0,053003 |
| | 1:10 | ns | 0,836335 |
| **COL I vs. FN** | 1:60 | * | 0,0139 |
| | 1:35 | ns | 0,0797 |
| | 1:10 | ns | 0,5564 |

descriptive statistics

| | **COL IV** | | | **COL I** | | | **FN** | | |
|---|---|---|---|---|---|---|---|---|---|
| | **1:60** | **1:35** | **1:10** | **1:60** | **1:35** | **1:10** | **1:60** | **1:35** | **1:10** |
| **N exp** | 3 | 3 | 3 | 3 | 3 | 3 | 3 | 3 | 3 |
| **Mean** | 0,2423 | 0,2087 | 0,302 | 0,1434 | 0,1393 | 0,2577 | 0,2228 | 0,2109 | 0,273 |
| SD | 0,02711 | 0,02709 | 0,1022 | 0,01287 | 0,02985 | 0,06234 | 0,03543 | 0,01165 | 0,1028 |

## fig S2E - pMCs MITF nuclear localization

stastical test

| Pass normality test? NO | | | |
|---|---|---|---|
| **Kruskal-Wallis** | | | |
| **Dunn's multiple comparisons test** | | | |
| | | **Significant?** | **P Value** |
| **COL IV** | COL IV 1:60 vs. COL IV 1:35 | ns | 0,2081 |
| | COL IV 1:60 vs. COL IV 1:10 | ns | >0,9999 |
| | COL IV 1:35 vs. COL IV 1:10 | ns | 0,3965 |
| **COL I** | COL I 1:60 vs. COL I 1:35 | * | 0,0186 |
| | COL I 1:60 vs. COL I 1:10 | ** | 0,0034 |
| | COL I 1:35 vs. COL I 1:10 | ns | >0,9999 |
| **FN** | FN 1:60 vs. FN 1:35 | ns | 0,7181 |
| | FN 1:60 vs. FN 1:10 | ns | >0,9999 |
| | FN 1:35 vs. FN 1:10 | ns | 0,2589 |
| **1:60** | COL I 1:60 vs. FN 1:60 | **** | <0,0001 |
| | COL I 1:60 vs. COL IV 1:60 | ** | 0,0056 |
| | FN 1:60 vs. COL IV 1:60 | ** | 0,0013 |
| **1:35** | COL I 1:35 vs. FN 1:35 | **** | <0,0001 |
| | COL I 1:35 vs. COL IV 1:35 | ** | 0,0046 |
| | FN 1:35 vs. COL IV 1:35 | **** | <0,0001 |
| **1:10** | COL I 1:10 vs. FN 1:10 | **** | <0,0001 |
| | COL I 1:10 vs. COL IV 1:10 | **** | <0,0001 |
| | FN 1:10 vs. COL IV 1:10 | *** | 0,0009 |

descriptive statistics

| | **COL IV** | | | **COL I** | | | **FN** | | |
|---|---|---|---|---|---|---|---|---|---|
| | **1:60** | **1:35** | **1:10** | **1:60** | **1:35** | **1:10** | **1:60** | **1:35** | **1:10** |
| **N exp** | 3 | 3 | 3 | 3 | 3 | 3 | 3 | 3 | 3 |
| **n cells** | 86 | 70 | 96 | 67 | 74 | 91 | 88 | 71 | 99 |
| **Mean** | 29,68 | 34,32 | 30,3 | 38,36 | 43,09 | 43,84 | 21,27 | 19,69 | 22,29 |
| SD | 12,05 | 15,48 | 11,44 | 11,58 | 11,34 | 10,83 | 7,844 | 7,228 | 9,502 |
| SEM | 1,299 | 1,85 | 1,168 | 1,415 | 1,318 | 1,135 | 0,8361 | 0,8578 | 0,955 |

## fig S3B - sholl profiles

stastical test

| Pass normality test? **YES** | | | |
|---|---|---|---|
| **Welch ANOVA tests** | | | |
| **Dunnett's T3 multiple comparisons test** | | | |
| | | **Significant?** | **P Value** |
| **COL IV** | COL IV 1:60 vs. COL IV 1:35 | ns | >0,9999 |
| | COL IV 1:60 vs. COL IV 1:10 | ns | 0,965 |
| | COL IV 1:35 vs. COL IV 1:10 | ns | 0,9489 |
| **COL I** | COL I 1:60 vs. COL I 1:35 | ns | 0,5182 |
| | COL I 1:60 vs. COL I 1:10 | ns | >0,9999 |
| | COL I 1:35 vs. COL I 1:10 | ns | 0,5964 |
| **FN** | FN 1:60 vs. FN 1:35 | ns | 0,8906 |
| | FN 1:60 vs. FN 1:10 | ns | 0,4342 |
| | FN 1:35 vs. FN 1:10 | ns | 0,7603 |

descriptive statistics

| | **COL IV** | | | **COL I** | | | **FN** | | |
|---|---|---|---|---|---|---|---|---|---|
| | **1:60** | **1:35** | **1:10** | **1:60** | **1:35** | **1:10** | **1:60** | **1:35** | **1:10** |
| **N exp** | 3 | 3 | 3 | 3 | 3 | 3 | 3 | 3 | 3 |
| **n cells** | 85 | 89 | 107 | 138 | 136 | 153 | 126 | 140 | 146 |
| **Area under the curve** | 258,2 | 259,2 | 249,3 | 148,9 | 132,1 | 149,6 | 303 | 318,5 | 340,1 |
| Std. Error | 28,97 | 27,3 | 24,41 | 14,97 | 15,55 | 20,01 | 30,29 | 29,88 | 29,15 |

## fig S4 - ratio cell area to % nuclear MITF

stastical test

| Pass normality test? NO | | | |
|---|---|---|---|
| **Kruskal-Wallis** | | | |
| **Dunn's multiple comparisons test** | | | |
| | | **Significant?** | **P Value** |
| **COL IV** | COL IV 1:60 vs. COL IV 1:35 | ns | >0,9999 |
| | COL IV 1:60 vs. COL IV 1:10 | ns | 0,5839 |
| | COL IV 1:35 vs. COL IV 1:10 | ns | >0,9999 |
| **COL I** | COL I 1:60 vs. COL I 1:35 | ns | 0,5497 |
| | COL I 1:60 vs. COL I 1:10 | *** | 0,0001 |
| | COL I 1:35 vs. COL I 1:10 | * | 0,0329 |
| **FN** | FN 1:60 vs. FN 1:35 | ns | >0,9999 |
| | FN 1:60 vs. FN 1:10 | *** | 0,0001 |
| | FN 1:35 vs. FN 1:10 | *** | 0,0001 |
| **1:60** | COL I 1:60 vs. FN 1:60 | **** | <0,0001 |
| | COL I 1:60 vs. COL IV 1:60 | **** | <0,0001 |
| | FN 1:60 vs. COL IV 1:60 | ** | 0,0014 |
| **1:35** | COL I 1:35 vs. FN 1:35 | **** | <0,0001 |
| | COL I 1:35 vs. COL IV 1:35 | **** | <0,0001 |
| | FN 1:35 vs. COL IV 1:35 | *** | 0,0006 |
| **1:10** | COL I 1:10 vs. FN 1:10 | **** | <0,0001 |
| | COL I 1:10 vs. COL IV 1:10 | **** | <0,0001 |
| | FN 1:10 vs. COL IV 1:10 | ns | 0,0603 |

descriptive statistics

| | **COL IV** | | | **COL I** | | | **FN** | | |
|---|---|---|---|---|---|---|---|---|---|
| | **1:60** | **1:35** | **1:10** | **1:60** | **1:35** | **1:10** | **1:60** | **1:35** | **1:10** |
| **N exp** | 3 | 3 | 3 | 3 | 3 | 3 | 3 | 3 | 3 |
| **n cells** | 67 | 47 | 93 | 81 | 67 | 83 | 78 | 82 | 75 |
| **Mean** | 61,63 | 62,14 | 62,59 | 21,29 | 16,54 | 12,92 | 136,2 | 132,9 | 75,83 |
| SD | 46,88 | 51,37 | 61,61 | 14,85 | 9,843 | 8,021 | 100,1 | 91,7 | 49,73 |
| SEM | 5,727 | 7,493 | 6,389 | 1,65 | 1,203 | 0,8804 | 11,34 | 10,13 | 5,742 |